Neutron Polarizabilities From Compton Scattering on the Deuteron?

Jonathan J. Karakowski and Gerald A. Miller

Department of Physics, Box 351560

University of Washington

Seattle, WA 98195-1560, U.S.A.

Abstract

A calculation of deuteron Compton scattering using non-relativistic perturbation theory is presented, with the primary motivation of investigating the feasibility of determining the neutron polarizabilities from this type of experiment. This calculation is expected to be valid for energies below 100 MeV. Pion-exchange, relativistic, and recoil corrections are also included. The low-energy theorem for gauge invariance is shown to be satisfied. The relative effects of the different terms and their effects on the determinations of the polarizabilities are discussed at energies of 49, 69, and 95 MeV. The cross-section is dominated by the seagull, polarizability, and electromagnetic multipole interactions. Relativistic and pion-exchange terms are also important, while recoil corrections and multipoles of $L=2$ and greater are negligible. The calculation provides a reasonable description of the experimental data points at 49 and 69 MeV. The polarizabilities are difficult to determine at these energies. A more accurate determination of the polarizabilities may be possible at 95 MeV.

1

I. INTRODUCTION

This paper is concerned with determining the polarizability of the neutron using Compton scattering from a deuteron. This is not a new idea and there have been previous calculations. However, advances on both the theoretical and experimental fronts invite the possibility of not only a more accurate calculation, but a more accurate measurement. The intent of this work is provide a complete potential model calculation.

A deuteron Compton scattering experiment was performed in 1994 [1], using 49 and 69 MeV photons, and experiments are in progress at Saskatoon [2] and Lund [3]. This has spurred recent activity. Brief articles by Wilbois, Wilhelm, and Arenhövel, [4] and L'vov and Levchuk [5,6] quote new theoretical results for Compton scattering. Calculations using effective field theory, based on the approach of Kaplan, Savage and Wise [7], have also been performed [8,9]. Another calculation [10], using an approach intermediate between ours and that of Ref. [8,9], is nearly complete.

Here is an outline of this paper. The remainder of this introduction reviews the concept of polarizability and examines the previous theoretical and experimental work. Descriptions of the methods used in the calculation are discussed in Sect. II. Checks which were performed to ensure the correctness of the work are also detailed there. The results of the numerical calculation are presented in Sect. III. The possibility of determining the neutron polarizabilities from deuteron Compton scattering is detailed. The conclusion and summary are in Sect. IV. Comparisons between our and previous calculations will be made in the summary. Some of the details of calculations omitted in the main text are in the Appendices. Complete formulae for all of the relevant scattering amplitudes may be found in the 1998 Ph. D. thesis [11] of one of the authors. This work is based on that thesis.

A. Background and Motivation

The symbol α is traditionally used to represent the electric polarizability, and β is used for the magnetic polarizability. The polarizability is the constant of proportionality between an external field and the average dipole moment that it induces. This induced moment in turn changes the potential energy of a system by an amount $\Delta E = -\frac{1}{2}\alpha E^2 - \frac{1}{2}\beta B^2$, known as the quadratic Stark effect. The nucleon polarizabilities are obtained using Hamiltonians for a dipole interacting with an external field: $H_{\text{int}} = -d_z E$, or $-\mu_z B$. Second order perturbation theory leads to

$$\alpha = 2\sum_{N'} \frac{|\langle\, N \mid d_z \mid N'\,\rangle|^2}{E_{N'} - E_N}, \quad \beta = 2\sum_{N'} \frac{|\langle\, N \mid \mu_z \mid N'\,\rangle|^2}{E_{N'} - E_N}. \tag{1}$$

We make an order-of-magnitude estimate of α by letting N' be an N^* state of mass 1440 MeV and taking the square of the matrix element to be about $\frac{1}{3}$fm^2. Then $\alpha \approx 13\times 10^{-4}$fm^3. This is of the same order as the currently accepted value of $\alpha \approx 12 \times 10^{-4}$fm^3. Hereafter the unit of polarizability will be 10^{-4}fm^3 .

The above expressions define the polarizability in terms of either an energy shift or an induced dipole moment. A third definition, which turns out to be the most practical, involves the scattering amplitude for elastic photon scattering, commonly known as Compton scattering. An initial photon, of laboratory four-momentum $(\omega_i, \vec{k}_i)$ and polarization vector $\hat{\epsilon}_{\lambda_i}$, where $\lambda_i = \pm 1$, is absorbed by a nucleon, which emits a final photon of four-momentum $(\omega_f, \vec{k}_f)$ and $\hat{\epsilon}_{\lambda_f}$. The angle between $\vec{k}_i$ and $\vec{k}_f$ is labeled θ, and the initial and final photon energies are related by $\omega_f = \omega_i/(1 + \frac{\omega_i}{m_N}(1 - \cos\theta))$. The scattering amplitude (to order ω^2) is given as [12]

$$f(\omega, \omega_i) = -\frac{e^2}{m_N}(\hat{\epsilon}^*_{\lambda_f} \cdot \hat{\epsilon}_{\lambda_i}) + (\omega_i + \omega_f)g(e, m_N, \kappa_N; \hat{k}_f, \hat{\epsilon}^*_{\lambda_f}, \hat{k}_i, \hat{\epsilon}_{\lambda_i}) +$$
$$\bar{\alpha}\omega_f\omega_i(\hat{\epsilon}^*_{\lambda_f} \cdot \hat{\epsilon}_{\lambda_i}) + \bar{\beta}\omega_f\omega_i(\hat{k}_f \times \hat{\epsilon}^*_{\lambda_f}) \cdot (\hat{k}_i \times \hat{\epsilon}_{\lambda_i}) +$$
$$\omega_f\omega_i h(e, m_N, \kappa_N; \hat{k}_f, \hat{\epsilon}^*_{\lambda_f}, \hat{k}_i, \hat{\epsilon}_{\lambda_i}). \tag{2}$$

The first term, the Thomson amplitude, is the dominant one at low energies. The internal structure becomes important only in second order. The terms with the angular dependence

$(\hat{\epsilon}^*_{\lambda_f} \cdot \hat{\epsilon}_{\lambda_i})$ and $(\hat{k}_f \times \hat{\epsilon}^*_{\lambda_f}) \cdot (\hat{k}_i \times \hat{\epsilon}_{\lambda_i})$ are written separately, and all other combinations of the four photon unit vectors are lumped together in the function h. The coefficients of these two terms are defined as the generalized polarizabilities $\bar{\alpha}$ and $\bar{\beta}$.

The generalized polarizabilities $\bar{\alpha}$, $\bar{\beta}$ are not the same as the static polarizabilities α, β. They are related by $\bar{\alpha} = \alpha + \Delta\alpha$, $\bar{\beta} = \beta + \Delta\beta$, where $\Delta\alpha, \Delta\beta$ arise from terms in the scattering amplitude of the same energy and angular dependence as those of α, β. The first term in the explicit expression for $\Delta\alpha$ is [13,14] : $\Delta\alpha = \frac{e^2 r_e^2}{3m} + \frac{e^2(1+\kappa^2)}{4m^3}$, where r_e stands for the charge radius, and accounts for about 40% of $\bar{\alpha}_p$. This is only about a 5% effect in the neutron. The first term in $\Delta\beta$ is [14] $\Delta\beta = -\frac{e^2 e_c^2}{6m}$. Additional corrections involve the nucleon form factors $F_1(4m^2)$, $F_2(4m^2)$ and their derivatives [14].

Our primary interest is in determining polarizabilities through experiment, but it is useful to review the theoretical calculations. Baldin [15] obtained an estimate $4.0 \le \bar{\alpha}_p \le 15.0$, for the proton polarizabilities by including the first excited state $(N' = N + \pi)$. Gell-Mann and Goldberger [16] derived the once-subtracted dispersion relation for a forward scattering amplitude $f(\omega)$. The low energy limit of Eq. (2), along with the dispersion relation and the the optical theorem, leads to the Baldin sum rule [15]:

$$\bar{\alpha} + \bar{\beta} = \int_{m_\pi}^{\infty} \frac{\sigma_{\text{tot}}(\omega')d\omega'}{2\pi^2\omega'^2}, \tag{3}$$

where $\sigma_{\text{tot}}(\omega)$ is the total cross-section for photoabsorption. This relation provides a model-independent constraint on the possible values of $\bar{\alpha}$ and $\bar{\beta}$. The generally accepted results from the sum rule are [17,18] $\bar{\alpha}_p + \bar{\beta}_p = 14.3 \pm 0.5$, $\bar{\alpha}_n + \bar{\beta}_n = 15.8 \pm 0.5$. However, a recent experiment [19] predicts: $\bar{\alpha}_p + \bar{\beta}_p = 13.69 \pm 0.14$, $\bar{\alpha}_n + \bar{\beta}_n = 14.44 \pm 0.69$. The values for the proton are consistent with the older ones, but the new neutron values are slightly lower.

A dispersion relation for $\bar{\alpha} - \bar{\beta}$ can also be derived [20,21], but it contains a contribution that depends on the amplitudes for $\gamma\gamma \to \pi\pi$, which are not well known. Nevertheless, this difference has been estimated to be [22] $\bar{\alpha}_p - \bar{\beta}_p \approx 3.2$, $\bar{\alpha}_n - \bar{\beta}_n \approx 3.9$. Comparison with the sum rules above yield smaller values for the individual polarizabilities than the $\bar{\alpha}_p \approx 11$ and $\bar{\alpha}_n \approx 12$ measured experimentally.

4

Various quark models have also been used. A simple nonrelativistic model with a harmonic oscillator potential yields reasonable values for $\bar{\beta}$ but predicts $\bar{\alpha}_p > \bar{\alpha}_n$, so more sophisticated models are needed. For example, Werner and Weise [23] obtained $\bar{\alpha}$ and $\bar{\beta}$ using a valence quark core surrounded by a pion cloud to be $\bar{\alpha}_N \approx 7 - 9, \bar{\beta}_N \approx 2$. Perhaps the most promising new method is to use chiral perturbation theory. Calculations with only the one-loop contribution produce [24]: $\bar{\alpha}_N = 10\bar{\beta}_N \approx 13.6$. Including the next order as well as the effects of the Δ resonance gives [25,26] $\bar{\alpha}_p = 10.5 \pm 2.0$, $\bar{\alpha}_n = 13.4 \pm 1.5$, $\bar{\beta}_p = 3.5 \pm 3.6$, $\bar{\beta}_n = 7.8 \pm 3.6$. If we compare these two calculations with the Baldin sum rule, we find agreement for the predictions for the proton. However, the earlier calculation gives better agreement for the neutron than the higher-order one. The most important contributions to $\bar{\alpha}$ come from polarizing the pion cloud - about 50-70% [23]. The small value of $\bar{\beta} \approx 2$ can be attributed to cancellations between the large paramagnetic contribution from the Δ resonance (β) and the diamagnetic contribution from the pion cloud ($\Delta\beta$) [27].

Several experiments have been performed over the past few years with the aim of measuring nucleon polarizabilities. Most of these have specifically targeted the proton, with a differential cross-section for Compton scattering given (to order ω^2) as

$$\frac{d\sigma}{d\Omega} = \frac{d\sigma}{d\Omega}_{\text{Born}} - \frac{\alpha}{m_p}\left(\frac{\omega'}{\omega}\right)^2 \omega\omega' \left\{\frac{1}{2}(\bar{\alpha}_p + \bar{\beta}_p)(1 + \cos\theta)^2 + \frac{1}{2}(\bar{\alpha}_p - \bar{\beta}_p)(1 - \cos\theta)^2\right\}, \quad (4)$$

where α is the fine structure constant, and the Born term is that of Powell [28]. Note that the polarizability terms in equation (4) arise from interference between the polarizability amplitude of equation (2) and the Thomson amplitude. This formula shows the sensitivity of the cross-section to $\bar{\alpha}_p$ and $\bar{\beta}_p$ at different angles. The cross-section at forward angles is most sensitive to $\bar{\alpha}_p + \bar{\beta}_p$, while at backward angles only $\bar{\alpha}_p - \bar{\beta}_p$ can be measured. At 90° the β_p terms drop out completely. The expansion to order ω^2 is only valid to about 100 MeV [29]. Since the polarizability terms are of this order, too low an energy means that the cross-section is does not depend on $\bar{\alpha}_p$ and $\bar{\beta}_p$. Thus the optimal energy range for an experiment would be 70-100 MeV, which balances sensitivity with expansion validity.

A summary of a few proton Compton scattering experiments is given in Table I below.

The data are those of Moscow experiment [30], Illinois group [31], [32], and Mainz experiment [33]. More extensive reviews of these and other proton Compton scattering experiments can be found in the literature [12,29]. Despite some shortcomings, measurements for the polarizabilities in these experiments are in reasonable agreement with each other and with theoretical predictions. This is not the case for the neutron.

A direct neutron Compton scattering experiment would require the use of a neutron target to detect a very small cross section. Therefore Coulomb scattering and quasi-elastic Compton scattering from a neutron bound in the deuteron have been used. The large Coulomb field of a heavy nucleus can induce a large dipole moment. Two separate 1988 experiments, both using ^{208}Pb as the target nucleus, quote large uncertainties: $\alpha_n = 12.0 \pm 10.0$, [34] $\alpha_n = 8.0 \pm 10.0$ [35] A more recent experiment by Schmiedmayer et al. [36], also using a lead target, produced $\alpha_n = 12.0 \pm 1.5 \pm 2.0$. This is the value normally quoted for the neutron electric polarizability. However, the accuracy of this result has been questioned [37,38]. It has been claimed that the uncertainties were underestimated, and that the best estimate for α_n is really $\sim 7 - 19$ [37]. An experiment to measure quasi-free Compton scattering by the neutron bound in the deuteron [39] was carried out by Rose et al. [40] in 1990, and obtained $\alpha_n = 11.7^{+4.3}_{-11.7}$. The uncertainties are large, but recent arguments indicate that this method is capable of producing more accurate results [41] and should be revisited.

It is clear that better experimental measurements of the neutron polarizability are needed. This is why we have chosen to investigate deuteron Compton scattering. This idea seems to have been originally suggested by Baldin [15], who calculated the cross-section in the impulse approximation. A more extensive calculation was undertaken by Weyrauch [42,43], but certain deficiencies to be discussed below, as well as a lack of emphasis on the neutron polarizability, suggest that this question can be reexamined.

II. DEUTERON COMPTON SCATTERING CALCULATIONS

The Feynman diagrams for several of the processes contributing to deuteron Compton scattering are shown in Fig. 1. The ovals at either end represent the deuteron wavefunctions, while the solid lines are the individual nucleons with which the photons (wavy lines) interact. Not all possible combinations are shown; interactions can occur on either nucleon with either an incoming or outgoing photon. Figure 1(a) is known as the seagull diagram, arising from the term in the Hamiltonian that is proportional to A^2. All other one-body interactions, which are at least of order ω^1, are represented by Fig. 1(b). These include the terms which depend on the polarizabilities α and β, as well as some relativistic corrections. Dispersive diagrams without meson exchange are depicted in Fig. 1(c)-(d). At lowest order, each vertex can be either an electric or magnetic multipole interaction. Our notation is that the intermediate state includes the effects of the un-denoted n-p interaction. Two of the meson-exchange effects which are included in this calculation are shown in Figure 1(e)-(f). The term of Figure 1(f) is called the "vertex correction".

A. Overview of Calculation

We begin with an overview of the methods used in the calculation. The differential cross-section will be calculated non-relativistically, to second order in the electric charge, using Fermi's golden rule. The transition matrix $\mathcal{T}_{fi}$ is then given by

$$\mathcal{T}_{fi} = \langle d_f, \vec{P}_f, \gamma_f \mid H^{\text{int}} \mid d_i, \vec{P}_i, \gamma_i \rangle + \sum_{C, \vec{P}_C} \frac{\langle d_f, \vec{P}_f, \gamma_f \mid H^{\text{int}} \mid C, \vec{P}_C \rangle \langle C, \vec{P}_C \mid H^{\text{int}} \mid d_i, \vec{P}_i, \gamma_i \rangle}{E_{d_i} + P_i^2/2m_d + \hbar\omega_i - E_C - P_C^2/2m_d + i\varepsilon} + \cdots, \quad (5)$$

where the $\cdots$ represents the crossing term, see Eq. (A1). The notation $d_{i(f)}$ is meant to represent all quantum numbers needed to describe the initial (final) deuteron state, except for the center-of-mass momentum $\vec{P}$, which will be absorbed into a momentum-conserving delta function. C represents all possible intermediate states.

The most important terms we include are represented by a non-relativistic Hamiltonian:

$$H^{\text{int}} = \sum_{j=n,p} \left[\frac{e_j^2}{2m_j} A^2(\vec{x}_j) - \frac{e_j}{m_j} \vec{A}(\vec{x}_j) \cdot \vec{p}_j - \frac{e(1+\kappa_j)}{2m_j} \vec{\sigma}_j \cdot \left(\vec{\nabla}_j \times \vec{A}(\vec{x}_j) \right) - \right. \tag{6}$$

$$\frac{1}{2} \bar{\alpha}_j \left(\frac{\partial \vec{A}(\vec{x}_j)}{\partial t} \right)^2 - \frac{1}{2} \bar{\beta}_j \left(\vec{\nabla}_j \times \vec{A}(\vec{x}_j) \right)^2 + \frac{i f_\pi e_\pi}{m_\pi} \left(\vec{\sigma}_j \cdot \vec{A}(\vec{x}_j) \right) \left(\tilde{\tau}_j \cdot \tilde{\phi}(\vec{x}_j) \right) +$$

$$\left. \frac{f_\pi \hbar}{m_\pi} \left(\vec{\sigma}_j \cdot \vec{\nabla}_j \right) \left(\tilde{\tau}_j \cdot \tilde{\phi}(\vec{x}_j) \right) \right] + \frac{1}{\hbar^2} \int d^3 x \, e^2 A^2(\vec{x}) \left[\phi_+(\vec{x})\phi_-(\vec{x}) + \phi_-(\vec{x})\phi_+(\vec{x}) \right],$$

where the vector potential is given by

$$\vec{A}(\vec{x_j}) = \frac{1}{\sqrt{V}} \sum_{\vec{k},\lambda=\pm 1} \sqrt{\frac{2\pi\hbar}{\omega}} [a_k \hat{\epsilon}_\lambda e^{i\vec{k}\cdot\vec{x}_j} + a_k^\dagger \hat{\epsilon}_\lambda^* e^{-i\vec{k}\cdot\vec{x}_j}]. \tag{7}$$

The operators $a_{k,\lambda}^{(\dagger)}$ destroy (create) a photon with momentum $\vec{k}$ and polarization λ. Similarly, the pion field operator is given by

$$\phi_\pm(\vec{x}_j) = \sum_q \frac{\hbar}{\sqrt{V}} \sqrt{\frac{2\pi}{E_\pi}} \left(a_\mp e^{i\vec{q}\cdot\vec{x}_j} + a_\pm^\dagger e^{-i\vec{q}\cdot\vec{x}_j} \right). \tag{8}$$

Here, $a_\pm$ destroys a $\pi_\pm$. The tildes in the Hamiltonian indicate vectors in isospin space. The approximate Hamiltonian (7) includes the effects of electric and magnetic dipole interactions. As discussed in Sect. IIC below and in Ref. [11], higher multipole moments are included also.

The transition matrix is proportional to a momentum-conserving delta function. We remove this delta function and define the scattering amplitude $\mathcal{M}_{fi}$:

$$\mathcal{T}_{fi} = \frac{1}{V} \frac{2\pi\hbar}{\sqrt{\omega_i \omega_f}} \frac{\delta(\vec{P}_f + \vec{k}_f - \vec{P}_i - \vec{k}_i)}{V} \mathcal{M}_{fi}. \tag{9}$$

The differential cross-section is given by

$$\left(\frac{d\sigma}{d\Omega} \right)_{fi} = \left(\frac{\omega_f}{\omega_i} \right)^2 \frac{E_f}{m_d} \mid \mathcal{M}_{fi} \mid^2, \tag{10}$$

where $E_f = \omega_i + m_d - \omega_f$, m_d is the deuteron mass. The spin-averaged cross-section is computed by summing over the final and averaging over the initial polarizations.

B. Seagull Terms

Using the interaction Hamiltonian $H^{SG} = \frac{e^2}{2m_p} A^2(\vec{x_p})$ accounts for the seagull diagram. The resulting contribution to the transition matrix is given by

$$\mathcal{M}_{fi}^{SG} = \frac{\sqrt{12\pi}e^2}{m_p}(\hat{\epsilon}_{\lambda_f}^* \cdot \hat{\epsilon}_{\lambda_i})(-1)^{1-M_f} \times \tag{11}$$

$$\left[\begin{pmatrix} 1 & 0 & 1 \\ -M_f & 0 & M_f \end{pmatrix} Y_{00}^*(\hat{q}) \; (I_0^{00} + I_0^{22})\delta_{M_f,M_i} + \right.$$

$$\left. \begin{pmatrix} 1 & 2 & 1 \\ -M_f & M_f - M_i & M_i \end{pmatrix} Y_{2,M_f-M_i}^*(\hat{q})(I_2^{02} + I_2^{20} - \frac{I_2^{22}}{\sqrt{2}}) \right],$$

where $\vec{r} \equiv \vec{x}_p - \vec{x}_n$, and

$$I_L^{l'l} \equiv \int_0^\infty dr u_{l'}(r) j_L(\frac{qr}{2}) u_l(r). \tag{12}$$

The radial deuteron wavefunction is represented by $u_{0,2}$ in which $0, 2$ refer to the orbital angular momentum. We use the "B" wavefunctions of Ref. [44], but the numerical results do not depend on this choice.

The terms that depend on the nucleon polarizabilities are very similar to the seagull term. Their transition matrices are given by the following expressions:

$$\mathcal{M}_{fi}^{\alpha} = -\omega_f\omega_i\sqrt{12\pi}(\hat{\epsilon}_{\lambda_f}^* \cdot \hat{\epsilon}_{\lambda_i})(-1)^{1-M_f}(\alpha_p + \alpha_n) \times \tag{13}$$

$$\left[\begin{pmatrix} 1 & 0 & 1 \\ -M_f & 0 & M_f \end{pmatrix} Y_{00}^*(\hat{q})(I_0^{00} + I_0^{22})\delta_{M_f,M_i} + \right.$$

$$\left. \begin{pmatrix} 1 & 2 & 1 \\ -M_f & M_f - M_i & M_i \end{pmatrix} Y_{2,M_f-M_i}^*(\hat{q})(I_2^{02} + I_2^{20} - \frac{I_2^{22}}{\sqrt{2}}) \right],$$

$$\mathcal{M}_{fi}^{\beta} = -\omega_f\omega_i\sqrt{12\pi}\left[\left(\hat{k}_i \times \hat{\epsilon}_{\lambda_i}\right) \cdot \left(\hat{k}_f \times \hat{\epsilon}_{\lambda_f}^*\right) \right](-1)^{1-M_f}(\beta_p + \beta_n) \times$$

$$\left[\begin{pmatrix} 1 & 0 & 1 \\ -M_f & 0 & M_f \end{pmatrix} Y_{00}^*(\hat{q})(I_0^{00} + I_0^{22})\delta_{M_f,M_i} + \right.$$

$$\left. \begin{pmatrix} 1 & 2 & 1 \\ -M_f & M_f - M_i & M_i \end{pmatrix} Y_{2,M_f-M_i}^*(\hat{q})(I_2^{02} + I_2^{20} - \frac{I_2^{22}}{\sqrt{2}}) \right]. \tag{14}$$

C. Dispersive Terms

Most of the remaining terms to be calculated are the dispersive terms, which are second-order in the interaction Hamiltonian. The contribution of the dispersive term to the transition matrix has the form

$$\mathcal{T}_{fi}^{disp} = \sum_{C,\vec{P}_C} \left\{ \frac{\langle\, d_f, \vec{P}_f, \gamma_f \mid H^{\mathrm{int}} \mid C, \vec{P}_C\,\rangle\langle\, C, \vec{P}_C \mid H^{\mathrm{int}} \mid d_i, \vec{P}_i, \gamma_i\,\rangle}{\hbar\omega_i + E_{d_i} - E_C - P_C^2/2m_d + i\varepsilon} + \right. \tag{15}$$

$$\left. \frac{\langle\, d_f, \vec{P}_f, \gamma_f \mid H^{\mathrm{int}} \mid C, \vec{P}_C, \gamma_i, \gamma_f\,\rangle\langle\, C, \vec{P}_C, \gamma_i, \gamma_f \mid H^{\mathrm{int}} \mid d_i, \vec{P}_i, \gamma_i\,\rangle}{-\hbar\omega_f + E_{d_i} - E_C - P_C^2/2m_d + i\varepsilon} \right\},$$

in which $H^{\mathrm{int}} = -\int \vec{J}(\vec{\xi})\cdot\vec{A}(\vec{\xi})d^3\xi$. We use $\vec{\xi}$ as a dummy variable, while $\vec{x}$ is a nucleon variable and $\vec{r}$ is a deuteron variable. The term $\vec{A}$ is handled using a multipole expansion:

$$\epsilon_\lambda e^{i\vec{k}\cdot\vec{\xi}} = \sum_{L=1}^{\infty}\sum_{M=-L}^{L} D_{M\lambda}^{(L)}(0,-\vartheta,-\varphi)i^L\sqrt{\frac{2\pi(2L+1)}{L(L+1)}}\times \tag{16}$$

$$\left\{ -\frac{i}{\omega}\vec{\nabla}_\xi\left(1+\xi\frac{d}{d\xi}\right)j_L(\omega\xi)Y_{LM}(\hat{\xi}) - i\omega\vec{\xi}j_L(\omega\xi)Y_{LM}(\hat{\xi}) - \lambda\vec{L}Y_{LM}(\hat{\xi})j_L(\omega\xi)\right\},$$

where $D_{M\lambda}^{(L)}(0,-\vartheta,-\varphi)$ is the Wigner-d function (we use the convention of [45]) , which is the overlap of the state $\mid L\lambda\,\rangle$, rotated by the Euler angles $(0,-\vartheta,-\varphi)$, with the state $\mid LM\,\rangle$. To simplify the notation, we define functions Φ_i and Φ_f by

$$\frac{1}{\sqrt{V}}\sqrt{\frac{2\pi\hbar}{\omega_i}}\hat{\epsilon}_{\lambda_i}e^{i\vec{k}_i\cdot\vec{\xi}} = \vec{\nabla}\Phi_i(\vec{\xi}) + \cdots, \tag{17}$$

$$\frac{1}{\sqrt{V}}\sqrt{\frac{2\pi\hbar}{\omega_f}}\hat{\epsilon}_{\lambda_f}^* e^{-i\vec{k}_f\cdot\vec{\xi}} = \vec{\nabla}\Phi_f(\vec{\xi}) + \cdots. \tag{18}$$

The gradient terms above correspond to the first term in the brackets of Eq. (16); see also Eqs. (A2) and (A3). In the low-energy limit, $\Phi_i(\vec{\xi}) \to \vec{\xi}\cdot\hat{\epsilon}_{\lambda_i}$, so $e\Phi$ is responsible for the electric dipole interaction.

Since $\vec{A}$ contains both a Φ and a non-Φ term, each H^{int} is the sum of two terms and then there are four different possibilities for each term of Eq. (15). The largest term, which includes an electric dipole $E1$ interaction at both $N\gamma$ vertices, is the one for which both matrix elements contain Φ. It is calculated in detail in Appendix A, and certain aspects

of it will also be discussed in this section. All terms in which one of the matrix elements contain Φ are calculated and tabulated in Appendix G of Karakowski's thesis [11]. These include all magnetic and spin-induced interactions occurring at exactly one vertex. Most of the terms that do not contain Φ are very small; see Appendix G of Ref. [11].

The largest second-order terms are the ones in which $-\int \vec{J}(\vec{\xi}) \cdot \vec{\nabla}\Phi(\vec{\xi})d^3\xi$ is substituted for all four H^{int}'s in Eq. (15). To avoid using an explicit expression for $\vec{J}$, we integrate by parts and use current conservation:

$$\vec{\nabla} \cdot \vec{J}(\vec{\xi}) = -\frac{i}{\hbar}\left[H, \rho(\vec{\xi})\right], \quad \rho(\vec{\xi}) = \sum_j e_j \delta(\vec{\xi} - \vec{x}_j). \tag{19}$$

The integral over ξ can then be performed to give

$$H^{\text{int}} = -i[H, (e/\hbar)\Phi(\vec{x}_p)], \tag{20}$$

where H is now the full Hamiltonian. If we examine only the piece of this commutator containing the proton kinetic energy, we see that

$$H^{\text{int,p}} = -i\left[\frac{p_p^2}{2m_p}, (e/\hbar)\Phi(\vec{x}_p)\right] = -\frac{e}{m_p}\vec{p}_p \cdot \vec{A}(\vec{x}_p), \tag{21}$$

so the Φ commutators contain the operators responsible for E1 transitions.

We switch to the center-of-mass variables $\vec{p} \equiv (\vec{p}_p - \vec{p}_n)/2$ and $\vec{P} \equiv \vec{p}_p + \vec{p}_n$ when we evaluate the commutator with the full Hamiltonian. Defining the "internal" Hamiltonian $H^{np} \equiv \frac{p^2}{2m_p} + V$, we get for the Φ_i term

$$H^{\text{int}} = -\frac{e}{m_p}\vec{P} \cdot \hat{\epsilon}_{\lambda_i}e^{i\vec{k}_i \cdot \vec{r}/2}e^{i\vec{k}_i \cdot \vec{R}} - i\left[H^{np}, (e/\hbar)\Phi_i(\vec{r}/2)\right]e^{i\vec{k}_i \cdot \vec{R}}. \tag{22}$$

The term with the $\vec{P}$ operator will be called the "recoil correction"; its matrix elements are calculated in Appendix B. The substitution $\vec{x}_p = \vec{r}/2 + \vec{R}$ generates an exponential of the form $e^{i\vec{P} \cdot \vec{R}}$, which combines with other similar exponentials to create the momentum-conserving delta function of Eq. (9). The net result of ignoring the recoil operators, therefore, is to replace $\vec{x}_p$ by $\vec{r}/2$ and switch from $\mathcal{T}_{fi}$ to $\mathcal{M}_{fi}$.

The interesting physics is contained in the second term of Eq. (22). Plugging this into Eq. (15), we get

$$\mathcal{M}_{fi}^{a,\mathrm{uncr}} = -\sum_C \left\{ \frac{\langle\, d_f\,|\,[H^{np}, \hat{\Phi}_f]\,|\,C\,\rangle\langle\,C\,|\,[H^{np}, \hat{\Phi}_i]\,|\,d_i\,\rangle}{\hbar\omega_i + E_{d_i} - E_C - P_C^2/2m_d + i\varepsilon} - \right.$$
$$\left. \frac{\langle\, d_f\,|\,[H^{np}, \hat{\Phi}_f]\,|\,C\,\rangle\langle\,C\,|\,[H^{np}, \hat{\Phi}_i]\,|\,d_i\,\rangle}{\hbar\omega_i + E_{d_i} - E_C - P_C^2/2m_d + i\varepsilon} \right\}. \tag{23}$$

The dimensionless operators $\hat{\Phi}_i \equiv (e/\hbar)\Phi_i(\vec{r}/2)$ and $\hat{\Phi}_f \equiv (e/\hbar)\Phi_f(\vec{r}/2)$ have been introduced, and this term has been labeled with the superscript "a".

Since $|\,d_{i,f}\,\rangle$ and $|\,C\,\rangle$ are eigenstates of H^{np}, the commutators can be expanded and some cancellations with the denominator can be made. This generates four terms, after adding the crossed term of Eq. (15):

$$\mathcal{M}_{fi}^{a} = \mathcal{M}_{fi}^{a1} + \mathcal{M}_{fi}^{a2} + \mathcal{M}_{fi}^{a3} + \mathcal{M}_{fi}^{a4}, \tag{24}$$

where

$$\mathcal{M}_{fi}^{a1} = \left[\frac{(\hbar\omega_i)^2}{2m_d} - \hbar\omega_i \right]^2 \sum_C \frac{\langle\, d_f\,|\,\hat{\Phi}_f\,|\,C\,\rangle\langle\,C\,|\,\hat{\Phi}_i\,|\,d_i\,\rangle}{\hbar\omega_i - \frac{(\hbar\omega_i)^2}{2m_d} + E_{d_i} - E_C + i\varepsilon}, \tag{25}$$

$$\mathcal{M}_{fi}^{a2} = \left[\hbar\omega_f + \frac{(\hbar\omega_f)^2}{2m_d} \right]^2 \sum_C \frac{\langle\, d_f\,|\,\hat{\Phi}_i\,|\,C\,\rangle\langle\,C\,|\,\hat{\Phi}_f\,|\,d_i\,\rangle}{-\hbar\omega_f - \frac{(\hbar\omega_f)^2}{2m_d} + E_{d_i} - E_C + i\varepsilon}, \tag{26}$$

$$\mathcal{M}_{fi}^{a3} = \left[\hbar\omega_f + \frac{(\hbar\omega_f)^2}{2m_d} - \hbar\omega_i + \frac{(\hbar\omega_i)^2}{2m_d} \right] \langle\, d_f\,|\,\hat{\Phi}_f\hat{\Phi}_i\,|\,d_i\,\rangle, \tag{27}$$

$$\mathcal{M}_{fi}^{a4} = \frac{1}{2}\langle\, d_f\,|\,\left[\,[H^{np}, \hat{\Phi}_i], \hat{\Phi}_f\right] + \left[\,[H^{np}, \hat{\Phi}_f], \hat{\Phi}_i\right]\,|\,d_i\,\rangle. \tag{28}$$

The first two terms correspond to the Feynman diagram Figure 1(b) and (c), and includes the case where both vertices are E1 interactions. The third term is a small recoil correction, calculated in Appendix B. The final term is responsible for compliance to the low-energy theorems which result from demanding gauge invariance; see Section II E.

The evaluation of Eqs. (25,26) while more complex than the one-body terms, is straightforward except for the additional complications of the intermediate states and energy denominators. We can obtain a compact expression by first examining the algebraic representation of the Φ operator in the appendix, equations (A2) and (A3), and noting that it contains distinct angular and radial pieces, which we call O and J, respectively (suppressing the sums and related indices here for simplicity). Then we find the $\mathcal{M}_{fi}^{a1}$ term can be rewritten as

12

$$\mathcal{M}_{fi}^{a1} = \sum_{\hat{C}} \sum_{l=0,2} \sum_{l'=0,2} \langle\, l'11M_f \mid O_f \mid \hat{C}\,\rangle\langle\, \hat{C} \mid O_i \mid l11M_i\,\rangle \times$$

$$\int_0^\infty \int_0^\infty r\chi_f^{l'\hat{C}}(r)J_i(r)u_l(r)dr, \tag{29}$$

where the angular quantum numbers $(L_C S_C J_C M_C)$, are denoted collectively by $\hat{C}$. The energy denominators have been incorporated in the function $\chi_f^{l'\hat{C}}(r)$. All of the second-order terms can be reduced to the form of Eq. (29). We determine $\chi_f^{l'\hat{C}}(r)$ by solving

$$\left[\frac{d^2}{dr^2} + \frac{m_p}{\hbar^2}[E_0 - V_{\hat{C}}(r)] - \frac{L_C(L_C+1)}{r^2}\right]r\chi_f^{l'\hat{C}}(r) = \frac{m_p}{\hbar^2}\frac{u_{l'}(r)J_f(r)}{r}. \tag{30}$$

where $E_0 \equiv \hbar\omega_i - \frac{(\hbar\omega_i)^2}{2m_d} + E_{d_i}$. For $V_{\hat{C}}(r)$, we use the Reid93 np potential [46]. This is an ordinary, inhomogeneous, second-order differential equation. The boundary condition is that $\chi_f^{l'\hat{C}}(r)$ must be an outgoing spherical wave at large distances.

D. Relativistic Corrections

The major relativistic correction here is the spin-orbit effect. Corrections arising from boosting the final deuteron wavefunction into a moving frame are small here and neglected. The origin of the relativistic spin-orbit effect can be understood by examining the magnetic term in the Hamiltonian of Eq. (6):

$$H^M = \sum_{j=n,p} \frac{e(1+\kappa_j)}{2m_j}\vec{\sigma}_j \cdot \vec{B}(\vec{x}_j). \tag{31}$$

The relativistic correction to the magnetic field for an object moving with velocity $\vec{v}$ is $\vec{B} \to \vec{B} - \vec{v} \times \vec{E}$, which leads to a relativistic term in the Hamiltonian:

$$H^{RC} = -\sum_{j=n,p} \frac{e_j(1+2\kappa_j)}{4m_j}\vec{\sigma}_j \cdot \left(\vec{v}_j \times \vec{E}_j\right). \tag{32}$$

Only the proton gives a correction because of the factor e_j. The effects of Thomas precession are included. Since $\vec{v} \approx \vec{p}/m$ and $\vec{E} = \vec{\nabla}V(r) \sim \vec{r}$ for a central potential, the dot product above goes as $\vec{\sigma} \cdot \vec{L}$, where $\vec{L}$ is the orbital angular momentum. If we make the minimal substitution $\vec{p} \to \vec{p} - e\vec{A}$, and use $\vec{E} = -\frac{\partial\vec{A}}{\partial t}$, H^{RC} becomes

$$H^{RC} = \sum_{j=n,p} \frac{e(1+2\kappa_j)}{4m_j^2} e_j \vec{\sigma}_j \cdot \left[\vec{A}(\vec{x}_j) \times \frac{\partial}{\partial t} \vec{A}(\vec{x}_j) \right], \tag{33}$$

and the resulting correction to the scattering amplitude is given by

$$\mathcal{M}_{fi}^{RC} = \langle\, d_f \,| \frac{-ie^2}{4m_p^2} \vec{\sigma}_p \cdot (\hat{\epsilon}_{\lambda_f}^* \times \hat{\epsilon}_{\lambda_i})(\hbar\omega_f + \hbar\omega_i)(2\kappa_p + 1)e^{-i\vec{q}\cdot\vec{r}/2} \,|\, d_i \,\rangle. \tag{34}$$

E. Checking the Calculation

There are checks which can be performed to help ensure that certain parts of the calculation are correct. One involves the use of the optical theorem to calculate the total cross-section σ_{tot} for deuteron photodisintegration, $\gamma d \to np$. With our normalization conventions, the optical theorem is given by

$$\sigma_{\text{tot}} = \frac{4\pi}{\omega} \text{Im}\mathcal{M}_{\text{fi}}(\theta = 0), \tag{35}$$

in which $\mathcal{M}_{fi}$ is our Compton amplitude. Only the diagram of Fig. 1b enters here. However, all combinations of interactions at the two vertices must be included. In a 1964 paper, Partovi [47] calculated the contributions from each of these interactions at 3 different energies. The dominant term is the one in which there is an E1 interaction at each vertex. He called this cross-section "approximation A", and added the other terms one by one in successive approximations, until every term was included ("approximation I"). These results are reproduced in Table II, along with the corresponding cross-sections extracted from this calculation. There is reasonable agreement at all energies; any differences can be attributed to changes in the short-range parts of the potentials. The meanings of the approximations in Table II: Approximation A: E1 only; Approximation B: A + singlet M1; Approximation C: B + E2; Approximation D: C + triplet M1; Approximation E: D + spin induced triplet M1; Approximation F: E + spin induced triplet M2; Approximation G: F + spin induced triplet E1; Approximation H: G + retardation corrections to E1; Approximation I: H + all other terms.

14

We also compare these photodisintegration cross-sections with experimental data up to 100 MeV. This is shown in Fig. 2. A vertex correction (see Fig. 1f) that contributes to this process, and is responsible for dominant meson exchange correction [48] is also included in a second graph of the range 50–100 MeV. There is good agreement with the data. Our photodisintegration cross-section also reproduces the correct threshold behavior, including pion-exchange current effect, as described by Brown &Jackson [48].

Another important check is to ensure that the calculation is gauge invariant. Since the relativistic two-photon scattering amplitudes must have the form $\epsilon_i^\mu T_{\mu\nu} \epsilon_f^\nu$, the condition imposed by gauge invariance is that $k_i^\mu T_{\mu\nu} \epsilon_f^\nu = \epsilon_i^\mu T_{\mu\nu} k_f^\nu = 0$. An important consequence of this is what is usually referred to as the low-energy theorem. Friar [49] showed, assuming only gauge invariance, that the full Compton amplitude must go as

$$\mathcal{M} \to \frac{e^2}{m_d}(\hat{\epsilon}_f \cdot \hat{\epsilon}_i). \tag{36}$$

as the photon energy goes to zero. This result is non-trivial because it involves the target(deuteron) mass; at low-energy the seagull amplitude depends on the *proton* mass :

$$\mathcal{M}_{\mathrm{sg}} \to \frac{e^2}{m_p}(\hat{\epsilon}_f \cdot \hat{\epsilon}_i). \tag{37}$$

Therefore, all other terms, including meson-exchange terms, must exactly cancel half of the seagull amplitude at threshold. That this occurs is easy to show, if we ignore meson-exchange terms. The only term which survives in the low-energy limit, from Eq. (28), is

$$\mathcal{M}^{a4} = \frac{1}{2}\langle\, d_f \mid \left[[\frac{p^2}{m_p}, \hat{\Phi}_i], \hat{\Phi}_f \right] + \left[[\frac{p^2}{m_p}, \hat{\Phi}_f], \hat{\Phi}_i \right] \mid d_i \,\rangle, \tag{38}$$

where we have only included the kinetic energy part of H^{np}; the potential energy term is cancelled by meson-exchange currents and will be discussed shortly. The amplitude of Eq. (37) can easily be shown to satisfy Friar's low-energy theorem. Since $\vec{A} \to \hat{\epsilon}$ at threshold (the dipole approximation), the definition of $\hat{\Phi}_i$ Eqs. (17) and (18) implies that $\hat{\Phi}_i \to \frac{e}{\hbar}\frac{\vec{r}}{2} \cdot \hat{\epsilon}_i$, $\quad \hat{\Phi}_f \to \frac{e}{\hbar}\frac{\vec{r}}{2} \cdot \hat{\epsilon}_f$. Evaluating the commutators of Eq. (38) then yields

$$\mathcal{M}^{a4} \to -\frac{e^2}{2m_p}(\hat{\epsilon}_f \cdot \hat{\epsilon}_i), \tag{39}$$

which cancels half of the seagull term as required. Our numerical calculation reproduces this result. The differential cross-section in this figure includes all terms except meson-exchange terms, and is seen to approach the correct limiting value. This plot shows only the forward cross-section, but the low energy theorem is satisfied at all angles.

We now examine the effects of the meson-exchange currents that were previously neglected. Since the potential energy portion of the double commutator term (Eq. 38) has not yet been accounted for, we suspect that this must cancel the explicit meson-exchange terms at low energy. This is indeed the case, as shown by Arenhövel [50]. Fig. 3 shows the four pion-exchange diagrams which contribute and cancel the double-commutator V^{OPEP} term at threshold. These four terms and the double-commutator V^{OPEP} term are described in detail in in App. I of [11]. Fig. 4 shows a graph of the differential cross-section at $0°$ which includes only these 5 terms. It is exactly zero at threshold. This is true at all angles, not just in the forward direction. Gauge invariance has been satisfied without explicitly demanding it in the formulation of the problem. The cross-section can be seen to have an ω^4 dependence, which means that the amplitude goes like ω^2.

III. RESULTS AND DISCUSSION

We now compute the deuteron Compton scattering cross-sections at the three experimentally relevant three energies of 49 MeV, 69 MeV and 95 MeV.

A. Effects of Various Terms in Cross-Section

The first step is to study the contributions to the cross-section from the major interactions. They will be labeled as follows: SG: seagull term, EM: All interactions, except for recoil corrections, arising from the multipole decomposition of the vector potential as described in App. A here and App. G of [11]. These include all electric and magnetic dipoles, as well as the double commutator term needed to satisfy the low-energy theorem. π: All pion interactions pictured in Fig 3 which are needed to satisfy the low-energy theorem. These are

detailed in App. J of [11]. $\alpha + \beta$: polarizability terms. Unless otherwise specified, the values

for the polarizabilities are chosen as $\alpha_p = 10.9$, $\alpha_n = 12.0$, $\beta_p = 3.3$, $\beta_n = 2.0$, as determined

in [31,36]. These major terms MT are displayed in Fig. 5 and on the top of Fig. 6. The data

from [1] is displayed on all graphs at 49 and 69 MeV; no data have yet been published for 95

MeV. The seagull term alone provides a reasonable description of the data at 49 MeV, and

does no worse than all the terms together at 69 MeV. At low energy, the seagull term has

a $(1 + \cos^2 \theta)$ dependence. As the energy becomes higher, this dependence is maintained at

the forward angles, while the cross-section get increasingly smaller at the backward angles.

It is the dominant term at all energies under consideration. The EM terms raise the seagull

cross-section and become increasingly important as the photon energy rises. The π terms,

on the other hand, do not have a very large effect, even at 95 MeV. These terms exactly

cancel at threshold and continue to nearly cancel at higher energies.

These terms are collectively called the Major Terms (MT). They describe the data rea-

sonably well. The smaller corrections are: RC: The Relativistic Correction. CMC: Recoil

Corrections (from the Center-of-Mass operator), as calculated in Appendix B. This also in-

cludes only the largest correction. VC: γN Vertex Corrections, such as the one pictured in

Fig. 1(f). These are detailed in [11]. These terms produce significant effects only at 95 MeV.

A detailed examination of the EM shows that multipoles higher than $L = 1$ are unimportant

below 100 MeV.

B. Determining Polarizabilities from Deuteron Cross-Sections

Having displayed the major contributions, we now investigate the dependence of the

cross-section on the size of the neutron polarizabilities. Figs. 7- 9 show the effects of varying

the magnitudes of α_n and β_n. The α_n term has the same $(1 + \cos^2 \theta)$ dependence as the seagull

term at low energies, while the β_n term goes like $\cos \theta$, so that the magnetic polarizability

term gives no contribution at 90°. The largest effects for both terms occur at extreme forward

and backward angles, while the experimental data points are in the middle. Figs. 7 and 8

17

show the changes to the cross-section over the range of $\alpha_n = 12.0 \pm 4.0$ and $\beta_n = 2.0 \pm 4.0$, which is a range of variation that is slightly larger than the errors quoted in [36]. These illustrate the sensitivity to the size error. At 49 MeV the effects of varying the polarizabilities between the values of $\alpha_n = 8.0 - 12.0$ and $\beta_n = 2.0 - 6.0$, are very small compared with the experimental error bars. There are only two data points at 69 MeV, and one of these lies above our calculated cross-section. The data point at the greatest angle is also difficult to describe at 49 MeV. Other calculations show similar inconsistencies with these two points [4,6,8]. Looking at (Fig. 9), we see that using a lower α_n and a higher β_n than the accepted values provide the best description of these points.

We must keep in mind that the proton polarizabilities also have uncertainties, and they contribute to the deuteron cross-section just as much as the neutron. Another set of graphs as described above is given for α_p and β_p (Figs. 10 and 11) , using only the ranges as the actual experimental error given in [31]. The same trends stand out here, most notably that a smaller value of α and a larger value of β would provide a better description of the data points at the back angles. Using the uncertainties in neutron and proton polarizabilities would allow a perfect reproduction of the data.

The chance to determine polarizabilities looks more promising at 95 MeV, as shown in Figs. 8 and 11. The effects of the polarizabilities are larger, and the range of ± 4.0 probably will extend beyond the experimental error bars at angles such as 50° and 140°.

C. Sources of Error

We would like to study the effects of some of the smaller terms more closely. For each term we estimate the absolute error in the value α_n (we fix $\beta_n = 2.0$ in this section) caused by neglecting various effects. These are listed in Table III and shown in some figures. First, we examine the gauge invariant set of pion terms. The results in Table III show that the value α_n would be slightly underestimated at the forward angles and overestimated at backward angles, and would not be affected around 120°. The magnitude of this error is about the

same as the experimental error in the polarizability, so these effects need to be included to make an accurate determination of α_n. The effect is same at all energies because both the π terms and polarizability terms have an ω^2 dependence. The recoil (CMC) corrections would be difficult to see on any graph, and this is also shown in the table. The largest errors are actually at the lowest energies, indicating that these terms are of order ω^1. The small values for $\Delta\alpha_n$ at 95 MeV indicate that these terms can be neglected here.

The relativistic corrections (RC) (Fig. 12) are not a "small" correction: even at 49 MeV they would have to be included in a calculation to make an accurate determination of α_n. The amount of error that would be introduced by neglecting these terms is comparable to α_n itself at some angles.

We turn to the vertex corrections (VC) of Fig. 1f which are also necessary for an accurate estimate of the polarizability. Their effect is greater than the effects of the other pion terms combined. The errors decrease as energy increases, but even at 95 MeV the errors, particularly at middle angles, is at least as large as previous errors in polarizability determinations. At backward angles the effect seems to be independent of energy. See Fig. 13. Finally, we note that the effect of the uncertainly in the πN coupling constant f on computed values of the deuteron Compton scattering are very small.

D. Tensor-Polarized Deuteron Compton Scattering

Another interesting observable is the tensor-polarized deuteron Compton scattering cross-section. Chen [9] introduced the idea that the quantity

$$\left(\frac{d\sigma}{d\Omega}\right)_T = \frac{1}{4}\left[2\frac{d\sigma}{d\Omega}(M_i = 0) - \frac{d\sigma}{d\Omega}(M_i = 1) - \frac{d\sigma}{d\Omega}(M_i = -1)\right] \tag{40}$$

be studied because it isolates the importance of pion exchange terms in effective field theory treatments of deuteron Compton scattering. Fig. 14 shows that $\left(\frac{d\sigma}{d\Omega}\right)_T$, as obtained in our complete calculation has only a slight dependence on the polarizabilities, which are our primary interest. We display our results to facilitate future comparisons between potential-model and effective field theory calculations. In our approach, the contributions of magnetic

19

interactions (MI) and relativistic corrections (RC) are the dominant contributions to $\left(\frac{d\sigma}{d\Omega}\right)_T$. We define the pion-exchange terms to include any pions that give rise to the tensor force (and the $l = 2$ state) in the deuteron. However, to be more consistent with the calculation of [9] we now will include only one pion exchange in the pion terms and no pion exchanges in the magnetic terms. Therefore, the D-state deuteron wavefunction $u_2(r)$ will be set to zero in all terms except for the Thomson term and the D-state contributions to this term will be grouped with the pion-exchange terms. Defined in this way, the pion-exchange effects turn out to be less than about 0.5 nb/sr at all angles. The results for the magnetic interactions (MI) are shown in Fig. 15. These interactions include all of the dispersive terms of Eq. (A1) as well as the seagull term of Eq. (12) computed without the deuteron D-state. In addition, we show the effect of including the deuteron D-state in the calculation of the magnetic terms (but not the seagull term). This is a non-negligible effect. Finally, the relativistic correction (RC) is added (including the D-state). Since this is a spin-orbit effect, we group this with the magnetic interactions. Both the relativistic term and the deuteron D-states have a large effect in the calculation; this observable is very sensitive to these individual effects.

IV. CONCLUSION

We have presented a calculation of deuteron Compton scattering valid for energies less than 100 MeV. All terms that we believe to be important are included. The seagull, lowest-order multipoles, and polarizability effects dominate the cross-section. Relativistic corrections must also be incorporated in the calculation. Although smaller than the preceding terms, pion-exchange and vertex corrections are also needed to accurately determine the polarizabilities. We conclude that recoil effects and multipoles of second-order and higher are negligible in this energy range. We are able to achieve a reasonable agreement with the existing data; see Figs. 5,7 and 10.

This is the most extensive study so far of the effects of various terms in the cross-section on the value of α_n; see Tables III and IV. However, certain corrections which are

20

believed to be small have been omitted. No contributions from the Δ resonance have been explicitly included, although the magnetic polarizability itself is thought to contain a large paramagnetic contribution from the Δ. The Δ resonance has been shown to have a small effect on deuteron photodisintegration at energies less than 100 MeV [51]. In addition, considering the rather small contributions from π-exchange currents, heavier mesons such as the ρ have also been neglected. Higher-order relativistic corrections have not been included, but may need to be investigated further at energies near 100 MeV because of the large effects of the leading-order terms there.

The only fully detailed calculation of this type that has been published to date was by Weyrauch [42,43]. There are several important differences between his calculation and the present one. One of these is the NN potential used. He used a separable NN T matrix, while here we have found the Green's function for an intermediate NN state interacting via the Reid93 potential. He also assumes meson-exchange currents and relativistic corrections to be negligible. Probably the most important difference, however, is in gauge invariance. Gauge invariance is broken in the separable potential model and needs to be artificially restored. We have made no such assumptions here. Gauge invariance is a natural consequence of including all of the appropriate terms.

The cross-section predicted by Weyrauch is higher than the experimental data. However, recent results of Arenhövel [4] and Levchuk and L'vov [5,6] are in qualitative agreement with the data. Their work is similar to ours in that they also take diagrammatic approach using realistic potentials and including meson-exchange currents. The full details of their calculations are not yet available, so precise comparisons are not easily made. Lastly, a new calculation using effective field theories is also in qualitative agreement with the data [8]. We have also followed [9] in studying tensor-polarized Compton scattering. In our formulation the effects of the deuteron D-state and the relativistic correction are the dominant contribution.

We return to our basic question of the feasibility of making an accurate determination of the neutron polarizability from a deuteron Compton scattering experiment. The available

data at 49 and 69 MeV show that the ranges $\alpha_n = 12.0 \pm 4.0$ and $\beta_n = 2.0 \pm 4.0$ are reasonable, but a more accurate estimate is difficult since the polarizability terms are small relative to the experimental error bars. The uncertainties in the proton polarizabilities must also be taken into account. These problems are compounded by the data point at the greatest angle at each energy, which we all authors find difficult to describe. The closest description of all of the experimental data comes from lowering the value of α_n and raising β_n.

Perhaps the most promising estimates of the polarizability will come from data at higher energies. Assuming that the experimental error bars are not significantly larger, we should find that the range of polarizabilities that fit the data is smaller. Sensitivity to both α and β is largest at the forward and backward angles, while the cross-section at $90°$ is the least sensitive to the polarizabilities. Many of the "small" corrections, however, are particularly small at $120 - 140°$, and the cross-section is still very sensitive to the polarizabilities at these angles. The proton polarizabilities, unfortunately, will also make a larger contribution to the cross-section, and there is no way to determine the neutron polarizabilities more accurately than those of the proton in this experiment. This energy is at the limit of the validity of the low-energy expansion, which may introduce errors as well. In any case, studies at higher energies should provide additional information on the polarizabilities.

REFERENCES

[1] M. A. Lucas, PhD thesis, University of Illinois at Urbana-Champaign, 1994.

[2] D. Hornidge, to be published.

[3] B. Schroder, http://www.maxlab.lu.se.

[4] T. Wilbois, P. Wilhelm, and H. Arenhövel, Few-Body Systems Suppl. **9**, 263 (1995).

[5] M. I. Levchuk and A. I. L'vov, Few-Body Systems Suppl. **9**, 439 (1995).

[6] M. I. Levchuk and A. I. L'vov, nucl-th/9809034, 1998.

[7] D. B. Kaplan, M.J. Savage, and M.B. Wise, Nucl. Phys. **B478**, 629 (19960; Phys. Lett. **B424**, 390 (1998); nucl-th 9802075, to appear in Nucl. Phys. B.

[8] J.-W. Chen, H. W. Griesshammer, M. J. Savage, and R. P. Springer, nucl-th/9809023, 1998.

[9] J.-W. Chen, nucl-th/9810021.

[10] S.R. Beane, M. Malheiro, D.R. Phillips, U. van Kolck, 1999 preprint, UW@nt-99-7

[11] J. J. Karakowski, 1998 Ph. D. thesis; preprint nt@uw-99-5. nucl-th/9901011

[12] V. A. Petrunkin, Sov. J. Nucl. Phys. **12**(3), 278 (1981).

[13] V. A. Petrunkin, Nucl. Phys. **55**, 197 (1964).

[14] N. V. Maksimenko and S. G. Shulga, Sov. J. Nucl. Phys. **52**(2), 335 (1990).

[15] A. M. Baldin, Nucl. Phys. **18**, 310 (1960).

[16] M. Gell-Mann, M. L. Goldberger, and W. E. Thirring, Phys. Rev. **95**(6), 1612 (1954).

[17] M. Damashek and F. J. Gilman, Phys. Rev. D **1**(5), 1319 (1970).

[18] U. E. Schröder, Nucl. Phys. **B166**, 103 (1980).

[19] D. Babusci, G. Giordano, and G. Matone, Phys. Rev. C **57**(1), 291 (1998).

[20] J. Bernabeu, T. E. O. Ericson, and C. F. Fontan, Phys. Lett. **49B**(4), 381 (1974).

[21] J. Bernabeu and B. Tarrach, Phys. Lett. **69B**(4), 484 (1977).

[22] B. R. Holdstein and A. M. Nathan, Phys. Rev. D **49**(11), 6101 (1994).

[23] R. Weiner and W. Weise, Phys. Lett. **159B**(2), 85 (1985).

[24] V. Bernard, N. Kaiser, and U.-G. Meissner, Nucl. Phys. **B373**, 346 (1992).

[25] V. Bernard, N. Kaiser, and U.-G. Meissner, Physics Letters B **319**, 269 (1993).

[26] V. Bernard, N. Kaiser, U.-G. Meissner, and A. Schimdt, Z. Phys. A **348**, 317 (1994).

[27] N. Mukhopadhyay, A. Nathan, and L. Zhang, Phys. Rev. D **47**(1), R7 (1993).

[28] J. L. Powell, Phys. Rev. **75**, 32 (1949).

[29] A. M. Nathan, in *Chiral Dynamics: Theory and Experiment*, edited by A. M. Bernstein and B. R. Holstein, page 164, Springer, 1994.

[30] P. S. Baranov et al., Sov. J. Nucl. Phys. **21**(4), 355 (1975).

[31] F. Federspiel et al., Phys. Rev. Lett. **67**(12), 1511 (1991).

[32] B. E. MacGibbon et al., Phys. Rev. C **52**(4), 2097 (1995).

[33] A. Zieger et al., Phys. Lett. B **278**(34), 34 (1992).

[34] J. Schmiedmayer et al., Phys. Rev. Lett. **61**(9), 1065 (1988); J. Schmiedmayer et al. Nuclear Instruments and Methods A **284**, 137 (1989).

[35] L. Koester et al., Z. Phys. A **329**, 229 (1988).

[36] J. Schmiedmayer et al., Phys. Rev. Lett. **66**(8), 1015 (1991).

[37] T. L. Enik et al., Phys. of Atomic Nuclei **60**(4), 567 (1997).

[38] V. G. Nikolenko and A. B. Popov, Z. Phys. A **341**, 365 (1992).

[39] A. I. L'vov and V. A. Petrunkin, in *Perspectives on Photon Interactions with Hadrons and Nuclei*, edited by M. Schumacher and G. Tamas, page 123, Springer-Verlag, 1990.

[40] K. W. Rose et al., Phys. Lett. B **234**(4), 460 (1990).

[41] F. Wissmann, M. I. Levchuk, and M. Schumacher, Eur. Phys. J. A **1**, 193 (1998).

[42] M. Weyrauch, Phys. Rev. C **38**(2), 611 (1988).

[43] M. Weyrauch, Phys. Rev. C **41**(3), 880 (1990).

[44] R. Machleidt, Adv. Nucl. Phys. **19**, 189 (1989).

[45] M. E. Rose, *Elementary Theory of Angular Momentum*, New York, Wiley, 1957.

[46] V. G. J. Stoks et al., Phys. Rev. C **49**(6), 2950 (1994).

[47] F. Partovi, Ann. Phys. **27**, 79 (1964).

[48] G. E. Brown and A. D. Jackson, *The Nucleon-Nucleon Interaction*, North-Holland Pub. Co., 1976.

[49] J. L. Friar, Ann. of Phys. **75**, 179 (1975).

[50] H. Arenhövel, Z. Phys. A **297**, 129 (1980).

[51] S. Q. Ying, E. M. Henley, and G. A. Miller, Phys. Rev. C **38**, 1584 (1988).

TABLES

TABLE I. Experimental results for $\bar{\alpha}_p$ and $\bar{\beta}_p$

	ω_i(MeV)	θ(degrees)	result
Moscow(1975)	70-110	90,150	$\bar{\alpha}_p + \bar{\beta}_p = 5.8 \pm 3.3$
			$\bar{\alpha}_p - \bar{\beta}_p = 17.8 \pm 2.0$
Illinois (1991)	32-72	60,135	$\bar{\alpha}_p = 10.9 \pm 2.2 \pm 1.3$
			$\bar{\beta}_p = 3.3 \mp 2.2 \mp 1.3$
Mainz(1992)	98, 132	180	$\bar{\alpha}_p - \bar{\beta}_p = 7.03^{+2.49+2.14}_{-2.37-2.05}$
			$\bar{\alpha}_p = 10.62^{+1.25+1.07}_{-1.19-1.03}$
			$\bar{\beta}_p = 3.58^{+1.25+1.07}_{-1.19-1.03}$
Illinois/SAL(1995)	70-148	90,135	$\bar{\alpha}_p = 12.5 \pm 0.6 \pm 0.7 \pm 0.5$
			$\bar{\beta}_p = 1.7 \mp 0.6 \mp 0.7 \mp 0.5$

TABLE II. Comparison of photodisintegration cross-sections calculated in several approxima-tions. σ_P is the cross-section of Partovi [47], while σ_K is from this calculation.

Approximation	20 MeV		80 MeV		140 MeV	
	σ_P ($\mu b/sr$)	σ_K ($\mu b/sr$)	σ_P ($\mu b/sr$)	σ_K ($\mu b/sr$)	σ_P ($\mu b/sr$)	σ_K ($\mu b/sr$)
A	579.1	583.3	77.15	80.54	34.04	34.56
B	589.2	593.2	83.50	85.83	39.77	38.59
C	591.5	595.0	84.55	86.86	40.38	38.99
D	591.7	595.1	84.85	87.06	40.67	39.16
E	591.6	594.7	84.73	86.61	40.55	38.70
F	592.1	595.3	85.43	87.68	41.31	40.26
G	591.9	594.6	90.45	90.22	47.07	43.33
H	588.2	591.2	87.52	86.36	44.64	39.44
I	588.2	591.2	87.40	86.40	44.53	39.52

TABLE III. Error in electric polarizability generated by omitting the gauge-invariant set of pion terms π and the recoil corrections (CMC)

	π			CMC		
θ(deg)	49 MeV	69 MeV	95 MeV	49 MeV	69 MeV	95 MeV
0	-2.9	-2.6	-2.0	0.0	0.0	0.0
30	-2.7	-2.4	-1.9	-0.5	-0.2	-0.1
60	-2.1	-2.0	-1.6	-1.1	-0.5	-0.2
90	-1.2	-1.4	-1.7	0.1	0.2	0.3
120	0.0	-0.3	-0.9	1.4	0.8	0.5
150	1.1	0.9	0.5	0.6	0.3	0.2
180	1.5	1.4	1.1	0.0	0.0	0.0

TABLE IV. Error in electric polarizability generated by omitting the relativistic correction (RC) and vertex correction (VC)

	RC			VC		
θ(deg)	49 MeV	69 MeV	95 MeV	49 MeV	69 MeV	95 MeV
0	-7.9	-9.2	-11.9	3.7	1.4	0.9
30	-8.7	-10.2	-13.2	3.9	1.9	1.7
60	-9.7	-11.8	-15.8	3.7	2.7	4.1
90	-4.9	-7.1	-10.1	-1.1	1.2	5.0
120	5.1	4.1	3.4	-8.0	-3.4	0.9
150	10.0	9.8	10.3	-10.6	-5.9	-2.4
180	11.1	11.1	12.0	-11.1	-6.6	-3.3

FIGURES

FIG. 1. Feynman diagrams

FIG. 2. Total photodisintegration cross-sections compared with experimental data.

FIG. 3. Gauge invariant set of pion-exchange diagrams

FIG. 4. Forward differential cross-section including only pion-exchange and double-commutator V^{OPEP} contributions

FIG. 5. Contributions of different terms.

FIG. 6. Contributions of different terms at 95 MeV. Both major terms and smaller corrections are displayed

FIG. 7. Effect of varying α_n and β_n separately. $\beta_n = 2.0$ in the top graph and $\alpha_n = 12.0$ in the bottom.

FIG. 8. Effect of varying α_n and β_n separately at 95 MeV. α_n, β_n are as in Fig. 7

FIG. 9. Effect of varying both α_n and β_n .

FIG. 10. Effect of varying both α_p and β_p.

FIG. 11. Sensitivity to values of α, β at 95 MeV

FIG. 12. Effect of neglecting relativistic terms RC on the differential cross-section. The full calculation is labelled FC.

FIG. 13.   Effect of neglecting vertex corrections VC on the differential cross-section

FIG. 14.   Tensor-polarized deuteron Compton scattering cross-section, with and without polarizabilities. The values of $\alpha_n = 12.0$, $\beta_n = 2.0$, $\alpha_p = 10.9$, and $\beta_p = 3.3$ are used in the solid curve. All other interactions are included.

FIG. 15.   Tensor-polarized deuteron Compton scattering cross-section, including only magnetic interactions(MI). The dotted curve contains all of the dispersive terms, but only the contributions from the deuteron S-state are included. These contributions are added in the dashed curve. Relativistic corrections (RC) are added in the solid curve.

APPENDIX A: LEADING-ORDER DISPERSIVE TERMS

The remaining terms will be calculated using second-order perturbation theory:

$$\mathcal{T}_{fi}^{disp} = \sum_{C,\vec{P}_C} \left\{ \frac{\langle d_f, \vec{P}_f, \gamma_f \mid H^{\text{int}} \mid C, \vec{P}_C \rangle \langle C, \vec{P}_C \mid H^{\text{int}} \mid d_i, \vec{P}_i, \gamma_i \rangle}{\hbar\omega_i + E_{d_i} - E_C - P_C^2/2m_d + i\varepsilon} + \right. \tag{A1}$$
$$\left. \frac{\langle d_f, \vec{P}_f, \gamma_f \mid H^{\text{int}} \mid C, \vec{P}_C, \gamma_i, \gamma_f \rangle \langle C, \vec{P}_C, \gamma_i, \gamma_f \mid H^{\text{int}} \mid d_i, \vec{P}_i, \gamma_i \rangle}{-\hbar\omega_f + E_{d_i} - E_C - P_C^2/2m_d + i\varepsilon} \right\}.$$

Here C denotes the internal quantum numbers of the intermediate np state, and $\sum_C$ is shorthand for all sums and integrals which are needed to describe this complete set of states except for the center-of-mass states. These are written separately as $\vec{P}_C$. At this point, it is most convenient to use $H^{\text{int}} = -\int \vec{J}(\vec{\xi}) \cdot \vec{A}(\vec{\xi}) d^3\xi$, and then expand $\vec{A}$ into multipoles according to equation (16). There are 3 terms in this expansion; therefore, equation (A1) contains a total of 18 terms. The largest contributions at low energies (which we denote as $\mathcal{M}_{fi}^a$) arise from the gradient operator in Eq. (16). These are the leading-order contributions; the other terms are of order ω/m_N smaller. This gradient term includes the case where there is an $E1$ interaction at both γN vertices.

With this in mind, we define $\Phi_i(\vec{r})$ and $\Phi_f(\vec{r})$ by

$$\Phi_i(\vec{r}) \equiv -\frac{1}{\sqrt{V}} \sqrt{\frac{2\pi\hbar}{\omega_i}} \sum_{L=1}^{\infty} \sum_{M=-L}^{L} D_{M\lambda_i}^{(L)}(0,0,0) \frac{i^{L+1}}{\omega_i} \sqrt{\frac{2\pi(2L+1)}{L(L+1)}} \times \tag{A2}$$

30

$$\left(1 + r\frac{d}{dr}\right) j_L(\omega_i r) Y_{LM}(\hat{r})$$

$$\Phi_f(\vec{r}) \equiv \frac{1}{\sqrt{V}} \sqrt{\frac{2\pi\hbar}{\omega_f}} \sum_{L'=1}^{\infty} \sum_{M'=-L'}^{L'} (-1)^{L'-\lambda_f} D_{M'-\lambda_f}^{(L')}(0,-\theta,-\phi) \frac{i^{L'+1}}{\omega_f} \times$$

$$\sqrt{\frac{2\pi(2L'+1)}{L'(L'+1)}} \left(1 + r\frac{d}{dr}\right) j_{L'}(\omega_f r) Y_{L'M'}(\hat{r}), \tag{A3}$$

which means that

$$\frac{1}{\sqrt{V}} \sqrt{\frac{2\pi\hbar}{\omega_i}} \hat{\epsilon}_{\lambda_i} e^{i\vec{k}_i \cdot \vec{r}} = \vec{\nabla}_r \Phi_i(\vec{r}) + \cdots, \tag{A4}$$

$$\frac{1}{\sqrt{V}} \sqrt{\frac{2\pi\hbar}{\omega_f}} \hat{\epsilon}_{\lambda_f}^* e^{-i\vec{k}_f \cdot \vec{r}} = \vec{\nabla}_r \Phi_f(\vec{r}) + \cdots. \tag{A5}$$

After a lengthy calculation [11] one finds

$$\mathcal{M}_{fi}^a = \mathcal{M}_{fi}^{a1} + \mathcal{M}_{fi}^{a2} + \mathcal{M}_{fi}^{a3} + \mathcal{M}_{fi}^{a4}, \tag{A6}$$

where

$$\mathcal{M}_{fi}^{a1} = \frac{-2\pi e^2}{(\hbar\omega_i)(\hbar\omega_f)} \left[\frac{(\hbar\omega_i)^2}{2m_d} - \hbar\omega_i\right]^2 \sum_{l=0,2} \sum_{l'=0,2} \sum_{L,L'=1}^{\infty} \sum_{S_C=0,1} \sum_{J_C=|1-L|}^{1+L} \sum_{L_C=|J_C-S_C|}^{J_C+S_C} \times$$

$$i^{L+L'}(-1)^{L'-\lambda_f-M_f+J_C-M_i-\lambda_i} D_{M_f-M_i-\lambda_i,-\lambda_f}^{(L')}(0,-\theta,-\phi) \times$$

$$\sqrt{\frac{(2L+1)(2L'+1)}{LL'(L+1)(L'+1)}} \begin{pmatrix} 1 & L' & J_C \\ -M_f & M_f - M_i - \lambda_i & \lambda_i + M_i \end{pmatrix} \times$$

$$\begin{pmatrix} J_C & L & 1 \\ -\lambda_i - M_i & \lambda_i & M_i \end{pmatrix} \langle\, l'11\| Y_{L'} \|L_C S_C J_C\,\rangle \langle\, L_C S_C J_C\| Y_L \|l11\,\rangle \times$$

$$\int dr\, r\, u_l(r) \chi_f^{l'\hat{C}}(r) \psi_L(\frac{\omega_i r}{2}). \tag{A7}$$

We have used the definitions $E_0 \equiv \hbar\omega_i - \frac{(\hbar\omega_i)^2}{2m_d} - E_b$, and $\psi_L(x) \equiv j_L(x) + x\frac{d}{dx}j_L(x)$.

$$\mathcal{M}_{fi}^{a2} = \frac{-2\pi e^2}{(\hbar\omega_i)(\hbar\omega_f)} \left[\hbar\omega_f + \frac{(\hbar\omega_f)^2}{2m_d}\right]^2 \sum_{l=0,2} \sum_{l'=0,2} \sum_{L,L'=1}^{\infty} \sum_{S_C=0,1} \sum_{J_C=|1-L|}^{1+L} \sum_{L_C=|J_C-S_C|}^{J_C+S_C} \times$$

$$i^{L+L'}(-1)^{L'-\lambda_f+J_C-\lambda_i} D_{M_f-M_i-\lambda_i,-\lambda_f}^{(L')}(0,-\theta,-\phi) \sqrt{\frac{(2L+1)(2L'+1)}{LL'(L+1)(L'+1)}} \times$$

$$\begin{pmatrix} 1 & L & J_C \\ -M_f & \lambda_i & -\lambda_i + M_f \end{pmatrix} \begin{pmatrix} J_C & L' & 1 \\ \lambda_i - M_f & M_f - M_i - \lambda_i & M_i \end{pmatrix} \times$$

31

$$\langle\, l'11 \| Y_L \| L_C S_C J_C \,\rangle\langle\, L_C S_C J_C \| Y_{L'} \| l11 \,\rangle \times$$

$$\int dr\; r u_{l'}(r)\chi_f^{l\hat{C}}(r)\psi_L(\frac{\omega_i r}{2}), \tag{A8}$$

where $E_0' \equiv -\hbar\omega_f - \frac{(\hbar\omega_f)^2}{2m_d} - E_b$.

$$\mathcal{M}_{fi}^{a3} = -\frac{e^2\sqrt{\pi}}{(\hbar\omega_f)(\hbar\omega_i)}\left[\hbar\omega_f + \frac{(\hbar\omega_f)^2}{2m_d} - \hbar\omega_i + \frac{(\hbar\omega_i)^2}{2m_d}\right]\sum_{l=0,2}\sum_{l'=0,2}\sum_{\tilde{L}=|L-L'|}^{L+L'}\sum_{L=1}^{\infty}\sum_{L'=1}^{\infty}\times$$

$$D_{M_f-M_i-\lambda_i,-\lambda_f}^{(L')}(0,-\theta,-\phi)(2L+1)(2L'+1)\sqrt{\frac{2\tilde{L}+1}{LL'(L+1)(L'+1)}}\times$$

$$\begin{pmatrix} L & L' & \tilde{L} \\ 0 & 0 & 0 \end{pmatrix}\begin{pmatrix} L & L' & \tilde{L} \\ \lambda_i & M_f-M_i-\lambda_i & M_i-M_f \end{pmatrix}\begin{pmatrix} 1 & \tilde{L} & 1 \\ -M_f & M_f-M_i & M_i \end{pmatrix}\times$$

$$i^{L+L'}(-1)^{L'-\lambda_f-M_i}\langle\, l'11 \| Y_{\tilde{L}} \| l11 \,\rangle\int dr u_l(r)u_{l'}(r)\psi_{L'}(\frac{\omega_f r}{2})\psi_L(\frac{\omega_i r}{2}). \tag{A9}$$

The final term involves the double commutator of the Hamiltonian. The kinetic energy contribution is given here and potential energy below.

$$\mathcal{M}_{fi}^{a4,\text{KE}} = \frac{e^2\sqrt{\pi}}{m_p\omega_f\omega_i}\sum_{l=0,2}\sum_{l'=0,2}\sum_{\tilde{L}=|L-L'|}^{L+L'}\sum_{L=1}^{\infty}\sum_{L'=1}^{\infty}i^{L+L'}(-1)^{L'-\lambda_f-M_i}\times$$

$$(2L+1)(2L'+1)\sqrt{\frac{2\tilde{L}+1}{LL'(L+1)(L'+1)}}\begin{pmatrix} L & L' & \tilde{L} \\ 0 & 0 & 0 \end{pmatrix}\times$$

$$\begin{pmatrix} L & L' & \tilde{L} \\ \lambda_i & M_f-M_i-\lambda_i & M_i-M_f \end{pmatrix}\begin{pmatrix} 1 & \tilde{L} & 1 \\ -M_f & M_f-M_i & M_i \end{pmatrix}\times$$

$$D_{M_f-M_i-\lambda_i,-\lambda_f}^{(L')}(0,-\theta,-\phi)\langle\, l'11 \| Y_{\tilde{L}} \| l11 \,\rangle\times$$

$$\int dr\; u_l(r)u_{l'}(r)\left\{2\left[\frac{d}{dr}\psi_L(\frac{\omega_i r}{2})\right]\left[\frac{d}{dr}\psi_{L'}(\frac{\omega_f r}{2})\right] + \right.$$

$$\left.\frac{L(L+1)+L'(L'+1)-\tilde{L}(\tilde{L}+1)}{r^2}\psi_L(\frac{\omega_i r}{2})\psi_{L'}(\frac{\omega_f r}{2})\right\}. \tag{A10}$$

The other dispersive terms are listed in [11].

APPENDIX B: RECOIL CORRECTIONS

We will now return to the recoil corrections to the transition matrices which arise from the $\vec{P}$ operators in Eqs. (15)and (22) The main contributions from these terms are

$$\mathcal{T}_{fi}^{\mathrm{cm,uncr}} \equiv \tag{B1}$$

$$\sum_{C,\vec{P}_C} \frac{\langle\, d_f, \vec{P}_f \mid \frac{ie}{m_p}\vec{\nabla}\Phi_f(\frac{\vec{r}}{2})e^{-i\vec{k}_f\cdot\vec{R}} \cdot \vec{P} \mid C, \vec{P}_C\,\rangle\langle\, C, \vec{P}_C \mid \left[H^{np}, \hat{\Phi}_i\right]e^{i\vec{k}_i\cdot\vec{R}} \mid d_i, \vec{P}_i\,\rangle}{\hbar\omega_i + E_{d_i} - E_C - P_C^2/2m_d + i\varepsilon},$$

$$\mathcal{T}_{fi}^{\mathrm{cm,cr}} \equiv \tag{B2}$$

$$\sum_{C,\vec{P}_C} \frac{\langle\, d_f, \vec{P}_f \mid \frac{ie}{m_p}\vec{\nabla}\Phi_i(\frac{\vec{r}}{2})e^{i\vec{k}_i\cdot\vec{R}} \cdot \vec{P} \mid C, \vec{P}_C\,\rangle\langle\, C, \vec{P}_C \mid \left[H^{np}, \hat{\Phi}_f\right]e^{-i\vec{k}_f\cdot\vec{R}} \mid d_i, \vec{P}_i\,\rangle}{-\hbar\omega_f + E_{d_i} - E_C - P_C^2/2m_d + i\varepsilon}.$$

Since we are working in the lab frame, $\vec{P} \mid \vec{P}_i\,\rangle = 0$. We integrate the center-of-mass variables, use $\vec{A} = \vec{\nabla}\Phi$, and evaluate the commutator so that $\mathcal{T}_{fi}^{\mathrm{cm,uncr}}$ becomes:,

$$\mathcal{T}_{fi}^{\mathrm{cm,uncr}} = \sqrt{\frac{2\pi\hbar}{V\omega_f}}\frac{\delta(\vec{P}_i + \vec{k}_i - \vec{P}_f - \vec{k}_f)}{V}\left[\mathcal{T}_{fi}^{\mathrm{cm,uncr1}} + \mathcal{T}_{fi}^{\mathrm{cm,uncr2}}\right], \tag{B3}$$

where

$$\mathcal{T}_{fi}^{\mathrm{cm,uncr1}} = \sum_C \frac{\langle\, d_f \mid \frac{ie\hbar}{m_p}(\vec{k}_i \cdot \hat{\epsilon}_{\lambda_f}^*)e^{-\frac{i}{2}\vec{k}_f\cdot\vec{r}} \mid C\,\rangle\langle\, C \mid \left[\hbar\omega_i - \frac{(\hbar\omega_i)^2}{2m_d}\right]\hat{\Phi}_i \mid d_i\,\rangle}{\hbar\omega_i - \frac{(\hbar\omega_i)^2}{2m_d} + E_{d_i} - E_C + i\varepsilon},$$

$$\mathcal{T}_{fi}^{\mathrm{cm,uncr2}} = -\langle\, d_f \mid \frac{ie\hbar}{m_p}(\vec{k}_i \cdot \hat{\epsilon}_{\lambda_f}^*)e^{-\frac{i}{2}\vec{k}_f\cdot\vec{r}}\hat{\Phi}_i \mid d_i\,\rangle. \tag{B4}$$

Starting with $\mathcal{T}_{fi}^{\mathrm{cm,uncr1}}$, we do some algebra to obtain:

$$\mathcal{M}_{fi}^{\mathrm{cm,uncr1}} = -\sum_{l=0,2}\sum_{l'=0,2}\sum_{S_C=0,1}\sum_{J_C=|1-L|}^{1+L}\sum_{L_C=|J_C-S_C|}^{J_C+S_C}\sum_{L=1}^{\infty}\sum_{L'=0}^{\infty} \times \tag{B5}$$

$$(\hat{k}_i \cdot \hat{\epsilon}_{\lambda_f}^*)\frac{4\pi e^2}{m_p}\left[\hbar\omega_i - \frac{(\hbar\omega_i)^2}{2m_d}\right](-1)^{J_C-M_f-M_i-\lambda_i} \times$$

$$i^{L-L'}Y_{L',M_f-M_i-\lambda_i}^*(\hat{k}_f)\sqrt{\frac{2\pi(2L+1)}{L(L+1)}} \times$$

$$\langle\, l'11\| \, Y_{L'} \, \|L_C S_C J_C\,\rangle\langle\, L_C S_C J_C\| \, Y_L \, \|l11\,\rangle \times$$

$$\begin{pmatrix} 1 & L' & J_C \\ -M_f & M_f - M_i - \lambda_i & M_i + \lambda_i \end{pmatrix}\begin{pmatrix} J_C & L & 1 \\ -M_i - \lambda_i & \lambda_i & M_i \end{pmatrix} \times$$

$$\int_0^{\infty} r\, dr \chi_f^{l'\hat{C}}(r)\psi_L(\frac{\omega_i r}{2})u_l(r).$$

We list the results for the other $\mathcal{M}_{fi}^{\mathrm{cm}}$ terms:

$$\mathcal{M}_{fi}^{\mathrm{cm,uncr2}} = \sum_{l=0,2}\sum_{l'=0,2}\sum_{\tilde{L}=|L-L'|}^{L+L'}\sum_{L=1}^{\infty}\sum_{L'=0}^{\infty}(\hat{k}_i \cdot \hat{\epsilon}_{\lambda_f}^*)\frac{4\pi e^2}{m_p}(-1)^{M_i} \times \tag{B6}$$

$$i^{L-L'}Y^*_{L',M_f-M_i-\lambda_i}(\hat{k}_f)(2L+1)\sqrt{\frac{(2L'+1)(2\tilde{L}+1)}{2L(L+1)}} \times$$

$$\langle\, l'11\|\, Y_{\tilde{L}}\,\|l11\,\rangle \begin{pmatrix} L & L' & \tilde{L} \\ 0 & 0 & 0 \end{pmatrix}\begin{pmatrix} L & L' & \tilde{L} \\ \lambda_i & M_f-M_i-\lambda_i & M_i-M_f \end{pmatrix} \times$$

$$\begin{pmatrix} 1 & \tilde{L} & 1 \\ -M_f & M_f-M_i & M_i \end{pmatrix}\int_0^\infty dr\; u_{l'}(r)j_{L'}(\frac{\omega_f r'}{2})\psi_L(\frac{\omega_i r}{2})u_l(r),$$

$$\mathcal{M}^{\mathrm{cm,cr1}}_{fi} = \sum_{l=0,2}\sum_{l'=0,2}\sum_{S_C=0,1}\sum_{J_C=|1-L|}^{1+L}\sum_{L_C=|J_C-S_C|}^{J_C+S_C}\sum_{L'=1}^{\infty}\sum_{L=0}^{\infty} \times \tag{B7}$$

$$(\hat{k}_f\cdot\hat{\epsilon}_{\lambda_i})\frac{4\pi e^2}{m_p}\left[\hbar\omega_f + \frac{(\hbar\omega_f)^2}{2m_d}\right](-1)^{L'-\lambda_f-J_C} \times$$

$$i^{L+L'}\sqrt{\frac{(2L+1)(2L'+1)}{2L'(L'+1)}}D^{(L')}_{M'-\lambda_f}(0,-\theta,-\phi) \times$$

$$\langle\, l'11\|\, Y_L\,\|L_C S_C J_C\,\rangle\langle\, L_C S_C J_C\|\, Y_{L'}\,\|l11\,\rangle \times$$

$$\begin{pmatrix} 1 & L & J_C \\ -M_f & 0 & M_f \end{pmatrix}\begin{pmatrix} J_C & L' & 1 \\ -M_f & M_f-M_i & M_i \end{pmatrix} \times$$

$$\int_0^\infty r\, dr\chi^{l\hat{C}}_f(r)j_L(\frac{\omega_i r}{2})u_{l'}(r),$$

$$\mathcal{M}^{\mathrm{cm,cr2}}_{fi} = \sum_{\tilde{L}=|L-L'|}^{L+L'}\sum_{l=0,2}\sum_{l'=0,2}\sum_{L=0}^{\infty}\sum_{L'=1}^{\infty}(\hat{k}_f\cdot\hat{\epsilon}_{\lambda_i})\frac{2e^2}{m_p}(-1)^{L'-\lambda_f-M_i} \times \tag{B8}$$

$$i^{L+L'}(2L'+1)(2L+1)\sqrt{\frac{\pi(2\tilde{L}+1)}{2L'(L'+1)}}D^{(L')}_{M'-\lambda_f}(0,-\theta,-\phi) \times$$

$$\langle\, l'11\|\, Y_{\tilde{L}}\,\|l11\,\rangle \begin{pmatrix} L & L' & \tilde{L} \\ 0 & 0 & 0 \end{pmatrix}\begin{pmatrix} L & L' & \tilde{L} \\ 0 & M_f-M_i & M_i-M_f \end{pmatrix} \times$$

$$\begin{pmatrix} 1 & \tilde{L} & 1 \\ -M_f & M_f-M_i & M_i \end{pmatrix}\int_0^\infty dr\; u_{l'}(r)j_L(\frac{\omega_i r}{2})\psi_{L'}(\frac{\omega_f r}{2})u_l(r).$$

APPENDIX C: VERTEX CORRECTIONS

We calculate terms, such as the one shown in Fig. 1f,, in which a (γ,π) reaction on one nucleon is followed by the absorption of the pion on the second. This is followed (or

preceeded) by a photon emission from the second nucleon. These are vertex corrections to the "ordinary" second-order diagrams.

The result is
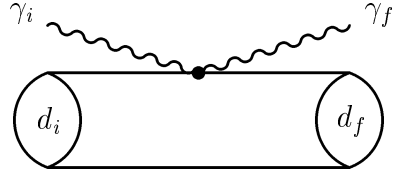
$$
\mathcal{M}_{fi}^{\pi\mathrm{vc}1} = -\sum_{l=0,2}\sum_{l'=0,2}\sum_{\tilde{J}=|1-J_C|}^{1+J_C}\sum_{J_C=|1-L''|}^{1+L''}\sum_{L''=|L-L'|}^{L+L'}\sum_{L=0}^{\infty}\sum_{L'=1}^{\infty}\sum_{i=-1,0,1}\sum_{j=-1,0,1}\times \tag{C1}
$$

$$
\frac{72\pi e^2 f^2\hbar^2\lambda_f\omega_f}{m_p m_\pi^2}i^{L+L'}(-1)^{L'-\lambda_f-M_f-M_i+j+J_C-L''}\left[\mu_p+(-1)^{L'}\mu_n\right]\times
$$

$$
D_{M'-\lambda_f}^{(L')}(0,-\theta,-\phi)(\hat{\epsilon}_{\lambda_i})_{-i}(2\tilde{J}+1)(2L+1)\sqrt{\frac{(L'+1)(2L''+1)(2J_C+1)}{4\pi}}\times
$$

$$
\begin{pmatrix} 1 & L' & J_C \\ -M_f & M_f-M_i-i & M_i+i \end{pmatrix}\begin{pmatrix} 1 & 1 & 1 \\ j & i & -i-j \end{pmatrix}\begin{pmatrix} 1 & L & L'' \\ 0 & 0 & 0 \end{pmatrix}\times
$$

$$
\begin{pmatrix} 1 & L & L'' \\ -j & 0 & j \end{pmatrix}\begin{pmatrix} 1 & L'' & \tilde{J} \\ i+j & -j & -i \end{pmatrix}\begin{pmatrix} J_C & \tilde{J} & 1 \\ -M_i-i & i & M_i \end{pmatrix}\times
$$

$$
\begin{Bmatrix} 0 & J_C & J_C \\ 1 & l & 1 \\ 1 & L'' & \tilde{J} \end{Bmatrix}\langle\,l'11\|\,[Y_{L'-1}\otimes t]_{L'}\,\|J_C 0 J_C\,\rangle\langle\,J_C\|\,Y_{L''}\,\|l\,\rangle\times
$$

$$
\int_0^{\infty}\int_0^{\infty}r\,dr\,r'\,dr'\,j_{L'-1}(\frac{\omega_f r'}{2})u_{l'}(r')G_{L_C}(r,r';E_0)j_L(\frac{\omega_i r}{2})\frac{d}{dr}\frac{e^{-m_\pi r/\hbar}}{r}u_l(r),
$$

where the Green's function $G_{L_C}(r,r';E_0)$ is defined by

$$
G_{L_C}(r,r';E_0) \equiv \langle r'\,|\,\frac{1}{E_0-H_{\hat{C}}^{np}+i\epsilon}\,|\,r\rangle. \tag{C2}
$$

The other correction terms are:

$$
\mathcal{M}_{fi}^{\pi\mathrm{vc}2} = -\sum_{l=0,2}\sum_{l'=0,2}\sum_{\tilde{J}=|1-J_C|}^{1+J_C}\sum_{J_C=|1-L''|}^{1+L''}\sum_{L''=|L-L'|}^{L+L'}\sum_{L=0}^{\infty}\sum_{L'=1}^{\infty}\sum_{i=-1,0,1}\sum_{j=-1,0,1}\times \tag{C3}
$$

$$
\frac{72\pi e^2 f^2\hbar^2\lambda_i\omega_i}{m_p m_\pi^2}i^{L+L'}(-1)^{L'+i+j-L''-M_f+J_C-M_i-\lambda_i}\left[\mu_p+(-1)^{L}\mu_n\right]\times
$$

$$
Y_{L'M'}^{*}(\hat{k}_f)(\hat{\epsilon}_{\lambda_f}^{*})_{-i}(2\tilde{J}+1)\sqrt{(L+1)(2L'+1)(2L''+1)(2J_C+1)}\times
$$

$$
\begin{pmatrix} 1 & L' & L'' \\ 0 & 0 & 0 \end{pmatrix}\begin{pmatrix} 1 & L' & L'' \\ -j & M_f-M_i-\lambda_i-i & M_i+\lambda_i+i+j-M_f \end{pmatrix}\times
$$

$$\begin{pmatrix} 1 & 1 & 1 \\ j & i & -i-j \end{pmatrix} \begin{pmatrix} 1 & L'' & \tilde{J} \\ i+j & M_f-M_i-\lambda_i-i-j & \lambda_i+M_i-M_f \end{pmatrix} \times$$

$$\begin{pmatrix} J_C & L & 1 \\ -M_i-\lambda_i & \lambda_i & M_i \end{pmatrix} \begin{pmatrix} 1 & \tilde{J} & J_C \\ -M_f & M_f-M_i-\lambda_i & M_i+\lambda_i \end{pmatrix} \times$$

$$\begin{Bmatrix} 1 & l' & 1 \\ 0 & J_C & J_C \\ 1 & L'' & \tilde{J} \end{Bmatrix} \langle\, J_C 0 J_C \|\, [Y_{L-1} \otimes t]_L\, \| l 1 1\,\rangle \langle\, l' \|\, Y_{L''}\, \| J_C\,\rangle \times$$

$$\int_0^\infty \int_0^\infty r\, dr\, r'\, dr'\, j_{L-1}\!\left(\frac{\omega_i r}{2}\right) u_l(r) G_{L_C}(r,r';E_0) j_{L'}\!\left(\frac{\omega_f r'}{2}\right)\frac{d}{dr'}\frac{e^{-m_\pi r'/\hbar}}{r'} u_{l'}(r'),$$
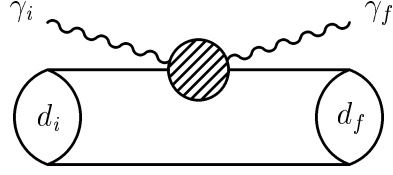
$$\mathcal{M}_{fi}^{\pi vc3} = -\sum_{l=0,2}\sum_{l'=0,2}\sum_{\tilde{J}=|1-J_C|}^{1+J_C}\sum_{J_C=|1-L''|}^{1+L''}\sum_{L''=|L-L'|}^{L+L'}\sum_{L=0}^{\infty}\sum_{L'=1}^{\infty}\sum_{i=-1,0,1}\sum_{j=-1,0,1} \times \qquad (C4)$$

$$\frac{72\pi e^2 f^2 \hbar^2 \lambda_f \omega_f}{m_p m_\pi^2} i^{L+L'}(-1)^{L'-\lambda_f+J_C+j+L''}\left[\mu_p + (-1)^{L'}\mu_n\right] \times$$

$$D^{(L')}_{M'-\lambda_f}(0,-\theta,-\phi)(\hat{\epsilon}_{\lambda_i})_{-i}(2\tilde{J}+1)(2L+1)\sqrt{\frac{(L'+1)(2L''+1)(2J_C+1)}{4\pi}} \times$$

$$\begin{pmatrix} J_C & L' & 1 \\ i-M_f & M_f-M_i-i & M_i \end{pmatrix} \begin{pmatrix} 1 & 1 & 1 \\ j & i & -i-j \end{pmatrix} \begin{pmatrix} 1 & L & L'' \\ 0 & 0 & 0 \end{pmatrix} \times$$

$$\begin{pmatrix} 1 & L & L'' \\ -j & 0 & j \end{pmatrix} \begin{pmatrix} 1 & L'' & \tilde{J} \\ i+j & -j & -i \end{pmatrix} \begin{pmatrix} 1 & \tilde{J} & J_C \\ -M_f & i & M_f-i \end{pmatrix} \times$$

$$\begin{Bmatrix} 1 & l' & 1 \\ 0 & J_C & J_C \\ 1 & L'' & \tilde{J} \end{Bmatrix} \langle\, J_C 0 J_C \|\, [Y_{L'-1} \otimes t]_{L'}\, \| l 1 1\,\rangle \langle\, l' \|\, Y_{L''}\, \| J_C\,\rangle \times$$

$$\int_0^\infty \int_0^\infty r\, dr\, r'\, dr'\, j_{L'-1}\!\left(\frac{\omega_f r'}{2}\right) u_l(r') G_{L_C}(r,r';E_0') j_L\!\left(\frac{\omega_i r}{2}\right)\frac{d}{dr}\frac{e^{-m_\pi r/\hbar}}{r} u_{l'}(r),$$
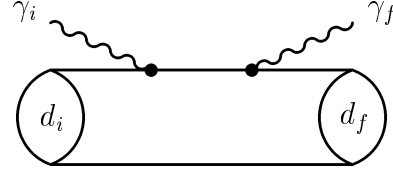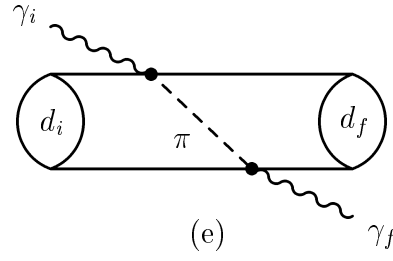
$$\mathcal{M}_{fi}^{\pi vc4} = -\sum_{l=0,2}\sum_{l'=0,2}\sum_{\tilde{J}=|1-J_C|}^{1+J_C}\sum_{J_C=|1-L''|}^{1+L''}\sum_{L''=|L-L'|}^{L+L'}\sum_{L=0}^{\infty}\sum_{L'=1}^{\infty}\sum_{i=-1,0,1}\sum_{j=-1,0,1} \times \qquad (C5)$$

$$\frac{72\pi e^2 f^2 \hbar^2 \lambda_i \omega_i}{m_p m_\pi^2} i^{L+L'}(-1)^{L'+i+j-L''+J_C-\lambda_i}\left[\mu_p + (-1)^{L}\mu_n\right] \times$$

$$Y^*_{L'M'}(\hat{k}_f)(\hat{\epsilon}^*_{\lambda_f})_{-i}(2\tilde{J}+1)\sqrt{(L+1)(2L'+1)(2L''+1)(2J_C+1)} \times$$

36

$$\begin{pmatrix} 1 & L' & L'' \\ 0 & 0 & 0 \end{pmatrix} \begin{pmatrix} 1 & L' & L'' \\ -j & M_f - M_i - \lambda_i - i & M_i + \lambda_i + i + j - M_f \end{pmatrix} \times$$

$$\begin{pmatrix} 1 & 1 & 1 \\ j & i & -i-j \end{pmatrix} \begin{pmatrix} 1 & L'' & \tilde{J} \\ i+j & M_f - M_i - \lambda_i - i - j & \lambda_i + M_i - M_f \end{pmatrix} \times$$

$$\begin{pmatrix} 1 & L & J_C \\ -M_f & \lambda_i & M_f - \lambda_i \end{pmatrix} \begin{pmatrix} J_C & \tilde{J} & 1 \\ \lambda_i - M_f & M_f - M_i - \lambda_i & M_i \end{pmatrix} \times$$

$$\begin{Bmatrix} 0 & J_C & J_C \\ 1 & l' & 1 \\ 1 & L'' & \tilde{J} \end{Bmatrix} \langle l'11 \| [Y_{L-1} \otimes t]_L \| J_C 0 J_C \rangle \langle J_C \| Y_{L''} \| l \rangle \times$$

$$\int_0^\infty \int_0^\infty r\, dr\, r'\, dr'\, j_{L-1}(\frac{\omega_i r}{2}) u_l(r') G_{L_C}(r, r'; E_0') j_{L'}(\frac{\omega_f r'}{2}) \frac{d}{dr'} \frac{e^{-m_\pi r'/\hbar}}{r'} u_l(r').$$

$$\begin{pmatrix} 1 & L' & L'' \\ 0 & 0 & 0 \end{pmatrix} \begin{pmatrix} 1 & L' & L'' \\ -j & M_f - M_i - \lambda_i - i & M_i + \lambda_i + i + j - M_f \end{pmatrix} \times$$

$$\begin{pmatrix} 1 & 1 & 1 \\ j & i & -i-j \end{pmatrix} \begin{pmatrix} 1 & L'' & \tilde{J} \\ i+j & M_f - M_i - \lambda_i - i - j & \lambda_i + M_i - M_f \end{pmatrix} \times$$

$$\begin{pmatrix} 1 & L & J_C \\ -M_f & \lambda_i & M_f - \lambda_i \end{pmatrix} \begin{pmatrix} J_C & \tilde{J} & 1 \\ \lambda_i - M_f & M_f - M_i - \lambda_i & M_i \end{pmatrix} \times$$

$$\begin{Bmatrix} 0 & J_C & J_C \\ 1 & l' & 1 \\ 1 & L'' & \tilde{J} \end{Bmatrix} \langle l'11 \| [Y_{L-1} \otimes t]_L \| J_C 0 J_C \rangle \langle J_C \| Y_{L''} \| l \rangle \times$$

$$\int_0^\infty \int_0^\infty r\, dr\, r'\, dr'\, j_{L-1}(\frac{\omega_i r}{2}) u_l(r') G_{L_C}(r, r'; E_0') j_{L'}(\frac{\omega_f r'}{2}) \frac{d}{dr'} \frac{e^{-m_\pi r'/\hbar}}{r'} u_l(r').$$

FIGURES

(a)

(b)   (c)

(d)   (e)

(f)

FIG. 1. Feynman diagrams

1

FIG. 2. Total photodisintegration cross-sections compared with experimental data.
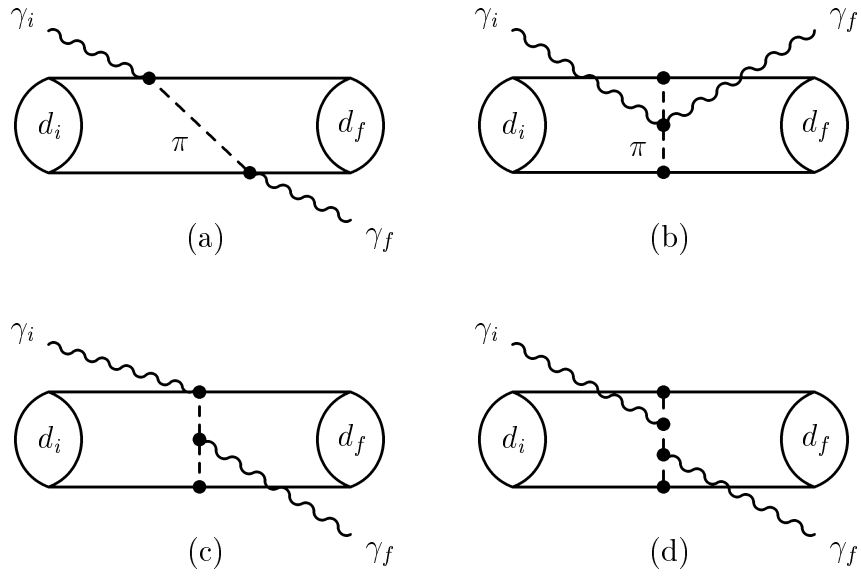
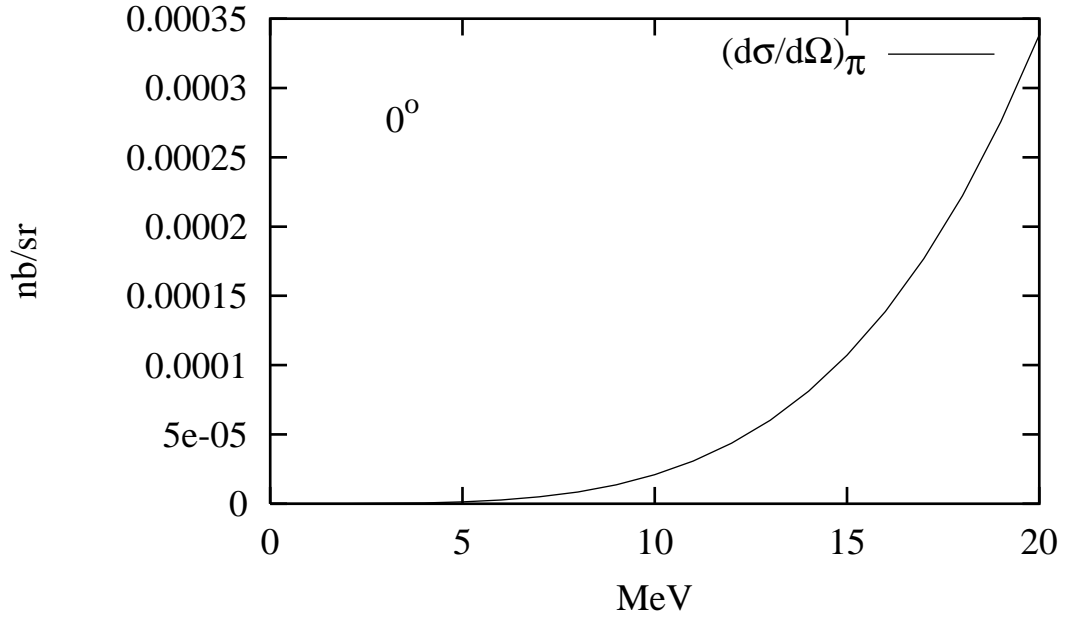FIG. 3. Gauge-invariant set of pion-exchange diagrams

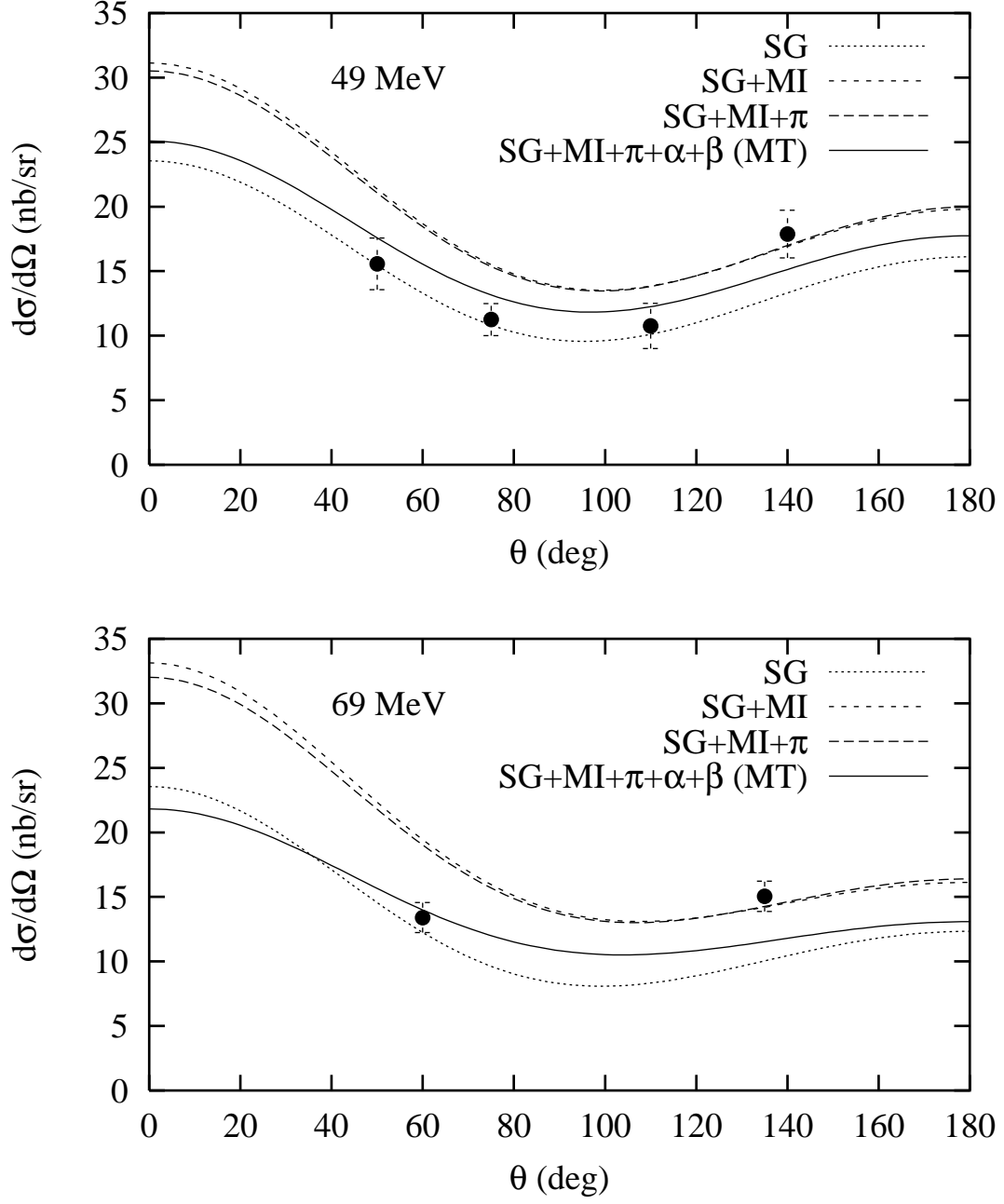FIG. 4. Forward differential cross-section including only pion-exchange and double commutator V^{OPEP} contributions
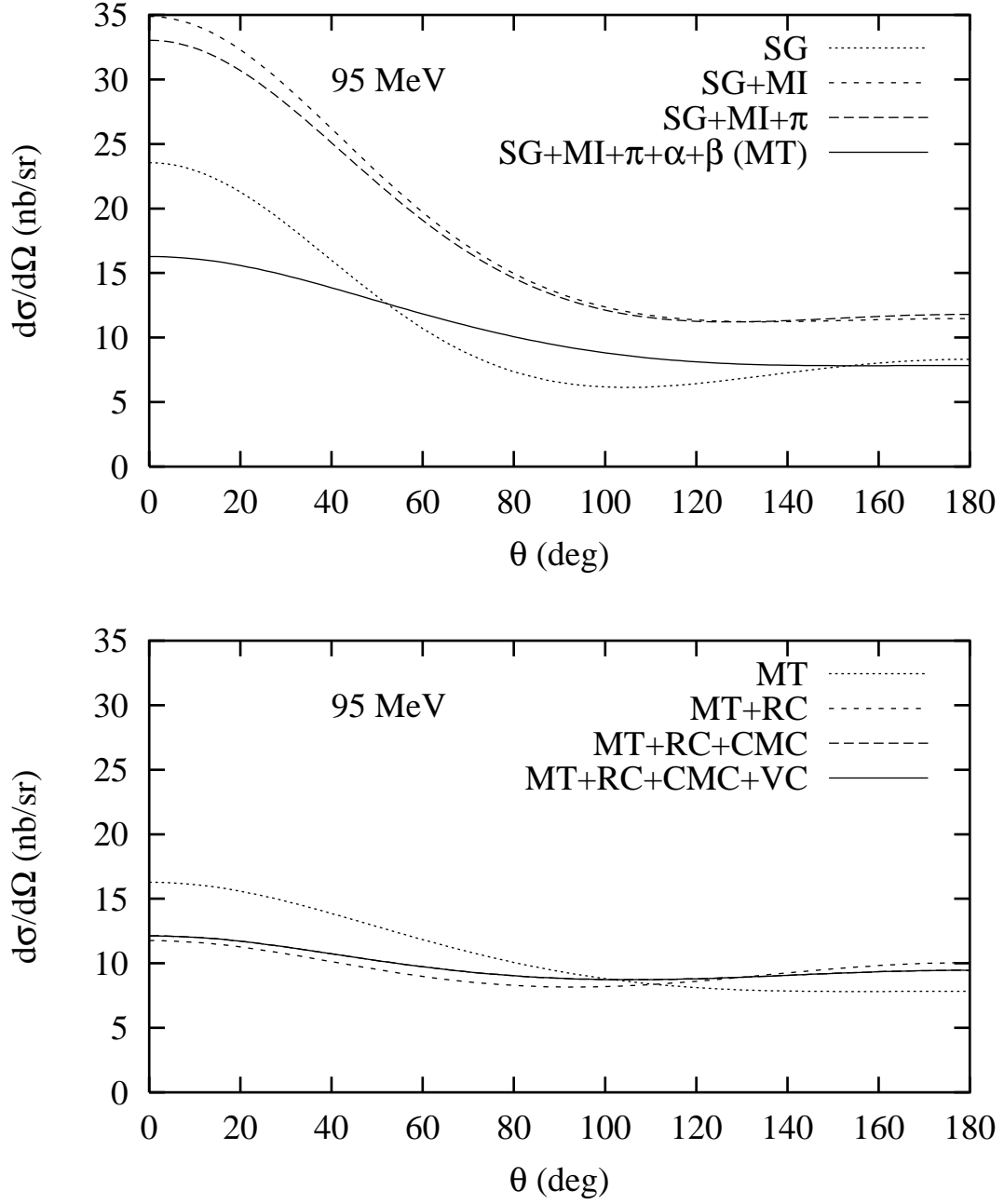
FIG. 5. Contributions of different terms.

FIG. 6. Contributions of different terms at 95 MeV. Both major terms and smaller corrections are displayed

FIG. 7. Effect of varying α_n and β_n separately. $\beta_n = 2.0$ in the top graph and $\alpha_n = 12.0$ in the bottom.

FIG. 8. Effect of varying α_n and β_n separately at 95 MeV. α_n, β_n are as in Fig. 7

FIG. 9. Effect of varying both α_n and β_n .

FIG. 10. Effect of varying both α_p and β_p.

FIG. 11. Sensitivity to values of α, β at 95 MeV

FIG. 12. Effect of neglecting relativistic terms on the differential cross-section. Our full calcu-laiton is labelled FC
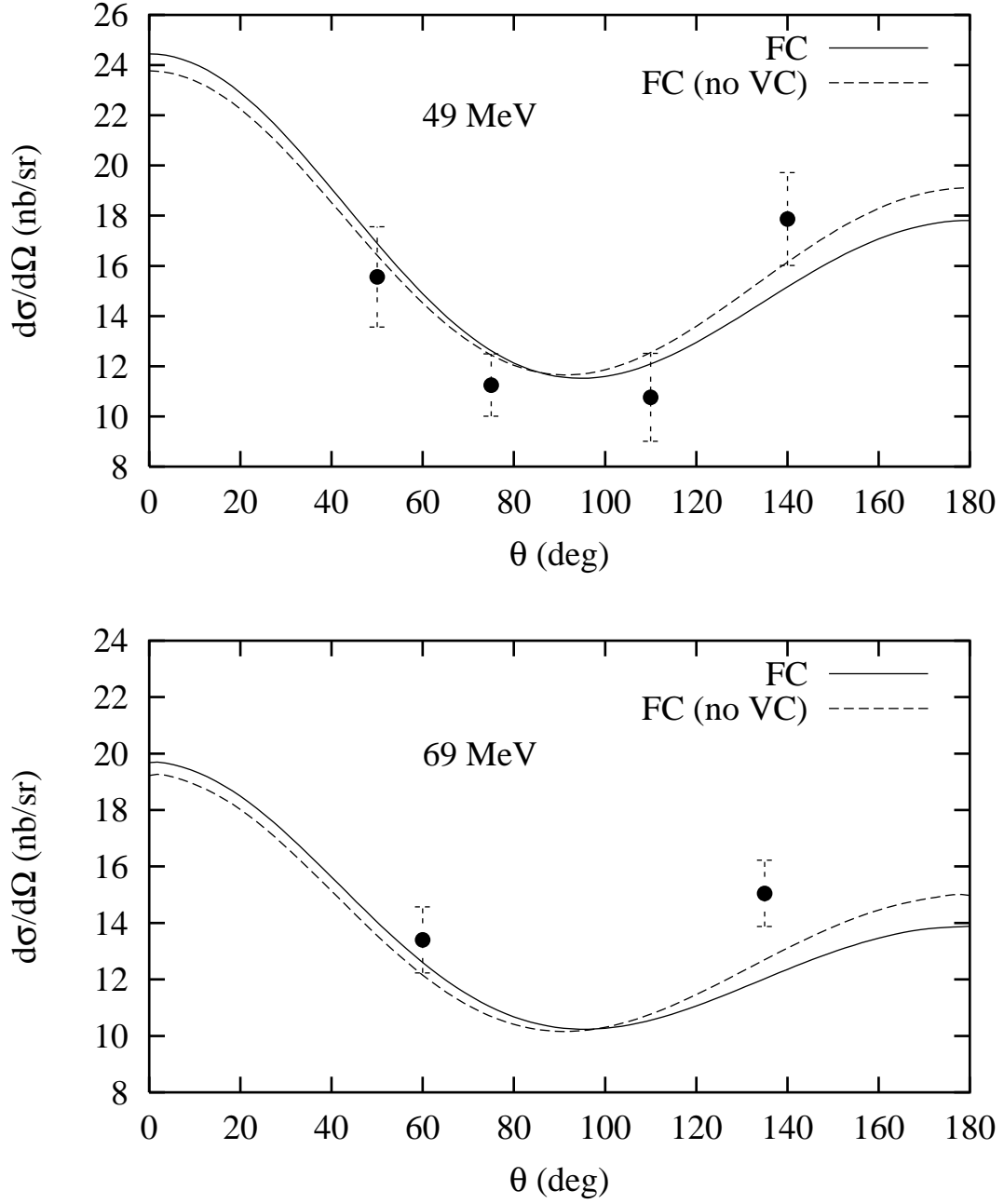
FIG. 13. Effect of neglecting vertex corrections VC on the differential cross-section
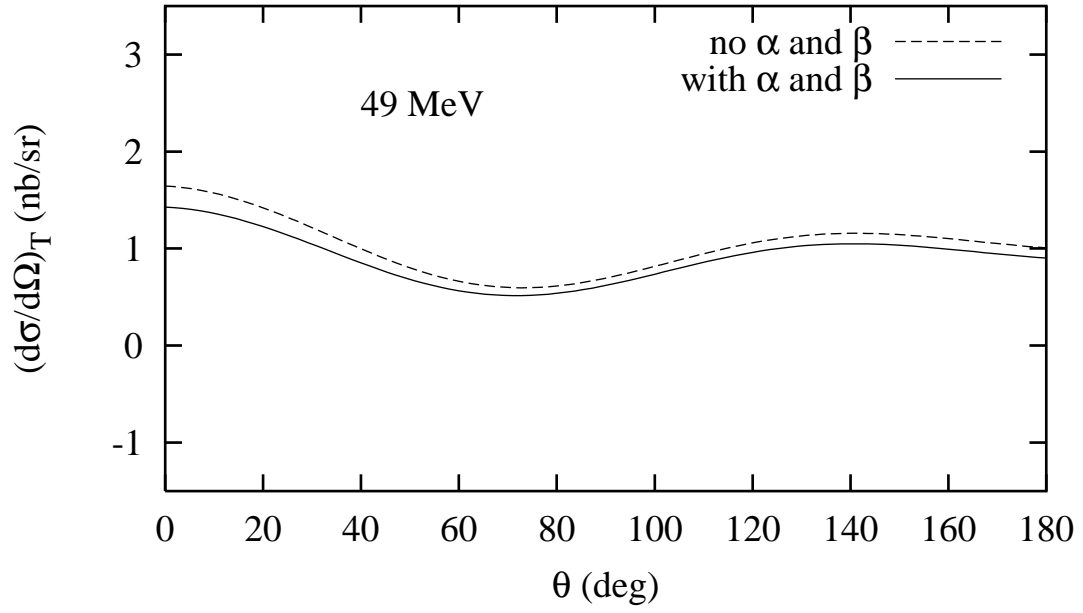
FIG. 14. Tensor-polarized deuteron Compton scattering cross-section, with and without polar-izabilities. The values of $\alpha_n = 12.0$, $\beta_n = 2.0$, $\alpha_p = 10.9$, and $\beta_p = 3.3$ are used in the solid curve. All other interactions are included.
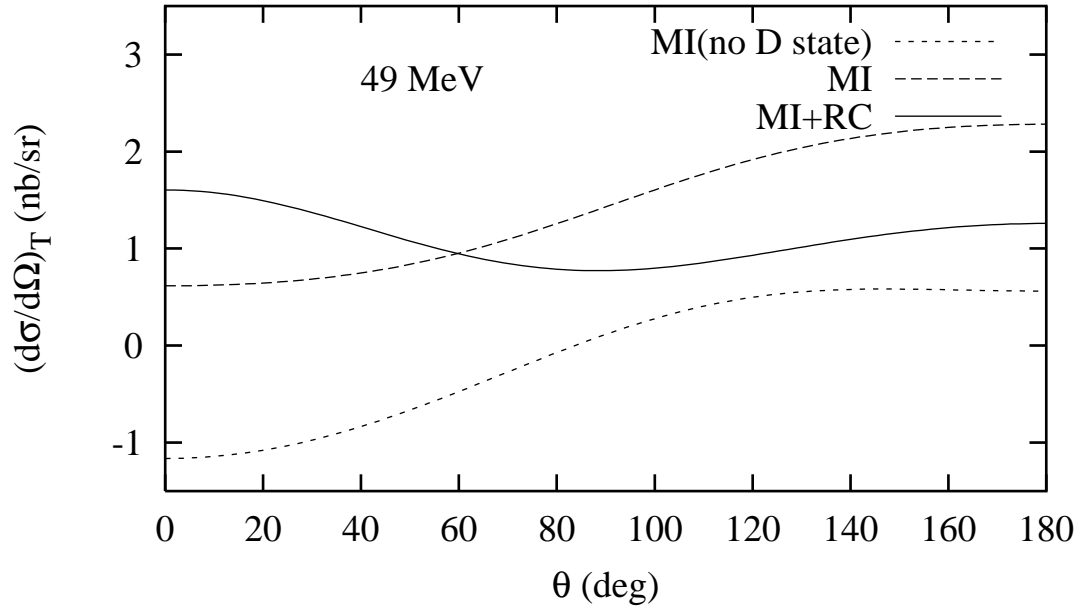
FIG. 15. Tensor-polarized deuteron Compton scattering cross-section, including only magnetic interactions(MI). The dotted curve contains all of the dispersive terms, , but only the contributions from the deuteron S-state are included. These contributions are added in the dashed curve. Relativistic corrections (RC) are added in the solid curve.